

Article

Comprehensive Second-Order Adjoint Sensitivity Analysis Methodology (2nd-ASAM) Applied to a Subcritical Experimental Reactor Physics Benchmark. VI: Overall Impact of 1st- and 2nd-Order Sensitivities on Response Uncertainties

Dan G. Cacuci ^{1,*}, Ruixian Fang ¹ and Jeffrey A. Favorite ²

¹ Center for Nuclear Science and Energy, Department of Mechanical Engineering, University of South Carolina, Columbia, SC 29208, USA; fangr@cec.sc.edu

² Los Alamos National Laboratory, Applied Physics (X) Division, MS F663, Los Alamos, NM 87545, USA; fave@lanl.gov

* Correspondence: cacuci@cec.sc.edu; Tel.: +1-803-777-9751

Received: 3 February 2020; Accepted: 22 March 2020; Published: 3 April 2020



Abstract: This work applies the Second-Order Adjoint Sensitivity Analysis Methodology (2nd-ASAM) to compute the 1st-order and unmixed 2nd-order sensitivities of a polyethylene-reflected plutonium (PERP) benchmark's leakage response with respect to the benchmark's imprecisely known isotopic number densities. The numerical results obtained for these sensitivities indicate that the 1st-order relative sensitivity to the isotopic number densities for the two fissionable isotopes have large values, which are comparable to, or larger than, the corresponding sensitivities for the total cross sections. Furthermore, several 2nd-order unmixed sensitivities for the isotopic number densities are significantly larger than the corresponding 1st-order ones. This work also presents results for the first-order sensitivities of the PERP benchmark's leakage response with respect to the fission spectrum parameters of the two fissionable isotopes, which have very small values. Finally, this work presents the overall summary and conclusions stemming from the research findings for the total of 21,976 first-order sensitivities and 482,944,576 second-order sensitivities with respect to all model parameters of the PERP benchmark, as presented in the sequence of publications in the Special Issue of *Energies* dedicated to "Sensitivity Analysis, Uncertainty Quantification and Predictive Modeling of Nuclear Energy Systems".

Keywords: polyethylene-reflected plutonium sphere; 1st- and 2nd-order sensitivities; isotopic number density; fission spectrum; expected value; variance and skewness of leakage response

1. Introduction

In Parts I–V [1–5], which are precursors of this work, the Second-Order Adjoint Sensitivity Analysis Methodology (2nd-ASAM) conceived by Cacuci [6–9] has been successfully applied to the subcritical polyethylene-reflected plutonium (acronym: PERP) metal fundamental physics benchmark [10] to compute the exact values of the sensitivities of the PERP's benchmark leakage response with respect to the PERP model parameters, as follows:

- (i) The 1st- and 2nd-order unmixed and mixed response sensitivities to the 180 group-averaged total microscopic cross sections [1];
- (ii) The 1st- and 2nd-order unmixed and mixed response sensitivities to the 21,600 group-averaged scattering microscopic cross sections [2];

- (iii) The 1st- and 2nd-order unmixed and mixed response sensitivities to the 120 fission process parameters [3];
- (iv) The 1st- and 2nd-order unmixed and mixed response sensitivities to the 10 source parameters [4]; and
- (v) The 2nd-order mixed response sensitivities involving the isotopic number densities and the other parameters of the PERP benchmark [5].

Although the geometrical dimensions and material composition of the PERP benchmark have been detailed in Part I [1], they are summarized for convenient reference in Table 1.

Table 1. Dimensions and material composition of the PERP benchmark.

Materials	Isotopes	Weight Fraction	Density (g/cm ³)	Zones
Material 1 (plutonium metal)	Isotope 1 (²³⁹ Pu)	9.3804×10^{-1}	19.6	Material 1 is assigned to zone 1, which has a radius of 3.794 cm.
	Isotope 2 (²⁴⁰ Pu)	5.9411×10^{-2}		
	Isotope 3 (⁶⁹ Ga)	1.5152×10^{-3}		
	Isotope 4 (⁷¹ Ga)	1.0346×10^{-3}		
Material 2 (polyethylene)	Isotope 5 (C)	8.5630×10^{-1}	0.95	Material 2 is assigned to zone 2, which has an inner radius of 3.794 cm and an outer radius of 7.604 cm.
	Isotope 6 (¹ H)	1.4370×10^{-1}		

As shown in Table 1, the six isotopic number densities correspond to each of the isotopes contained in the PERP benchmark, respectively. The isotopic number density is one of important parameters that contribute to the accuracy of the neutron transport calculation, as it appears in the total, scattering and fission macroscopic cross sections, as well as the source term of the neutron transport equation. The 1st-order and 2nd-order sensitivities of the leakage response with respect to the isotopic number densities will be computed by specializing the general expressions derived by Cacuci [6–8] to the PERP benchmark, and summarizing the respective contributions stemming from the total, scattering and fission macroscopic cross sections, and the sources, respectively. In addition, this work also presents results for the 1st-order sensitivities of the leakage response with respect to the fission spectrum parameters of the two fissionable isotopes, ²³⁹Pu and ²⁴⁰Pu, contained in the PERP benchmark.

The 2nd-order sensitivity analysis of the PERP benchmark is completed and concluded in this work, which is structured as follows: Section 2 presents the computational results for the six first-order sensitivities of the leakage response with respect to the benchmark's isotopic number densities. Section 3 presents the 6×6 second-order *unmixed* and *mixed* sensitivities of the leakage response solely with respect to the benchmark's isotopic number densities. Section 4 illustrates the impact of the 1st- and 2nd-order sensitivities on the uncertainties induced in the leakage response by the imprecisely known isotopic number densities. Section 5 reports the numerical results for the 60 first-order sensitivities to the fission spectrum. Finally, Section 6 highlights the overall conclusions arising from the pioneering computations presented in [1–5] and in this work of the 21,976 first-order sensitivities and 482,944,576 second-order sensitivities of the PERP benchmark's leakage response with respect to the imprecisely known model parameters of the PERP benchmark.

2. Computation of 1st-Order Sensitivities of the PERP Leakage Response to Isotopic Number Densities

As described in Part I [1], the neutron flux is computed by solving numerically the neutron transport equation using the PARTISN [11] multigroup discrete ordinates transport code with a spontaneous fission source provided by the code SOURCES4C [12] and employing the MENDF71X [13] 618-group cross sections collapsed to $G = 30$ energy groups, as detailed in [1]. For the PERP benchmark

under consideration, PARTISN [11] solves the following multi-group approximation of the neutron transport equation:

$$B^g(\alpha)\varphi^g(r, \Omega) = Q^g(r), \quad g = 1, \dots, G, \tag{1}$$

$$\varphi^g(r_d, \Omega) = 0, \Omega \cdot \mathbf{n} < 0, \quad g = 1, \dots, G, \tag{2}$$

where r_d denotes the external radius of the PERP benchmark, and where:

$$B^g(\alpha)\varphi^g(r, \Omega) \triangleq \Omega \cdot \nabla \varphi^g(r, \Omega) + \Sigma_t^g(r) \varphi^g(r, \Omega) - \sum_{g'=14\pi}^G \int \Sigma_s^{g' \rightarrow g}(r, \Omega' \rightarrow \Omega) \varphi^{g'}(r, \Omega') d\Omega' - \chi^g(r) \sum_{g'=14\pi}^G \int (\nu \Sigma_f)^{g'}(r) \varphi^{g'}(r, \Omega') d\Omega', \tag{3}$$

$$Q^g(r) \triangleq \sum_{k=1}^{N_f} \lambda_k N_{k,1} F_k^{SF} \nu_k^{SF} \left(\frac{2}{\sqrt{\pi} a_k^3 b_k} e^{-\frac{a_k b_k}{4}} \right) \int_{E^{g+1}}^{E^g} dE e^{-E/a_k} \sinh \sqrt{b_k E}. \tag{4}$$

The vector of model parameters $\alpha \triangleq [\sigma_t; \sigma_s; \sigma_f; \nu; \mathbf{p}; \mathbf{q}; \mathbf{N}]^\dagger$, which appears in Equation (1), has been defined in previous works [1–5] and is reproduced, for convenience, in Appendix A. The total neutron leakage from the PERP sphere is denoted [1–5] as $L(\alpha)$ and is defined [1–5] as follows:

$$L(\alpha) \triangleq \int_{S_b} dS \sum_{g=1}^G \int_{\Omega \cdot \mathbf{n} > 0} d\Omega \Omega \cdot \mathbf{n} \varphi^g(r, \Omega), \tag{5}$$

where S_b is the external surface area of the PERP ball.

Of course, $L(\alpha)$ depends on the imprecisely known model parameters through the neutron flux. For convenient reference, the histogram plot of the leakage for each energy group for the PERP benchmark is reproduced [1–4] in Figure 1. The value of the total leakage computed using Equation (5) for the PERP benchmark is 1.7648×10^6 neutrons/sec.

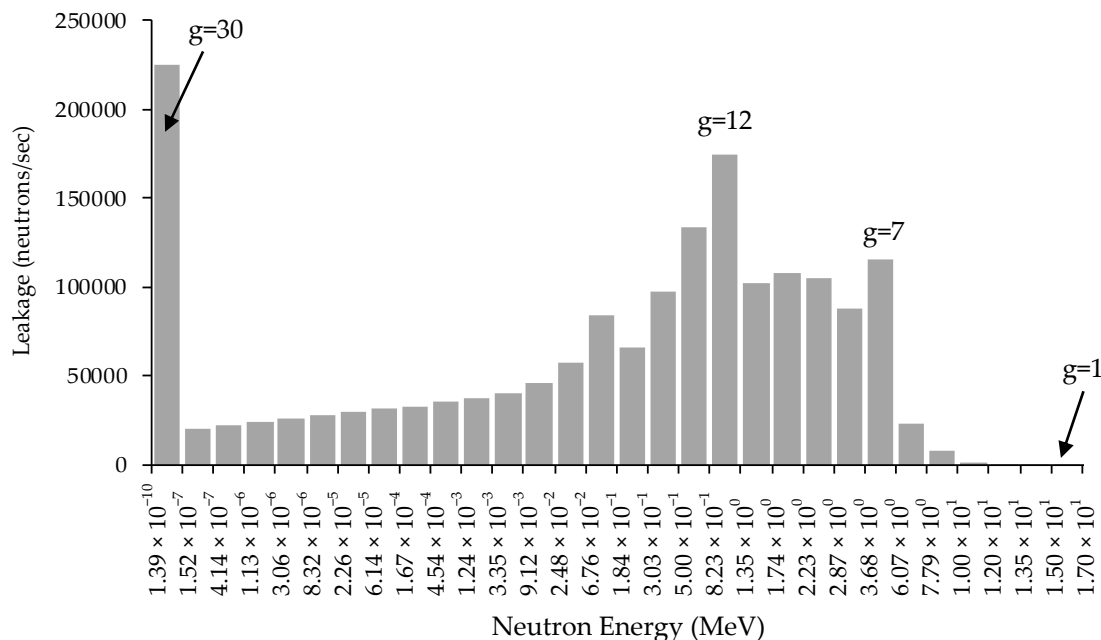


Figure 1. Histogram plot of the leakage for each energy group for the PERP benchmark.

The PERP benchmark comprises six isotopes ($I = 6$) and two materials ($M = 2$). Since the respective isotopes are all distinct materials, as specified in Table 1, it follows that only the following isotopic number densities exist for this benchmark: $N_{1,1}, N_{2,1}, N_{3,1}, N_{4,1}, N_{5,2}, N_{6,2}$, which implies that:

$$\mathbf{N} \triangleq [n_1, \dots, n_{J_n}]^\dagger \triangleq [N_{1,1}, N_{2,1}, N_{3,1}, N_{4,1}, N_{5,2}, N_{6,2}]^\dagger, \quad J_n = 6. \quad (6)$$

The isotopic number densities are components of the vectors \mathbf{t} , \mathbf{s} , \mathbf{f} and \mathbf{q} , respectively, as defined in Appendix A. Therefore, the vector of first-order sensitivity of the PERP leakage response to the isotopic number densities, which will be denoted as $\partial L(\boldsymbol{\alpha})/\partial \mathbf{N}$, comprises the following four components:

$$\frac{\partial L(\boldsymbol{\alpha})}{\partial n_j} = \left[\frac{\partial L(\boldsymbol{\alpha})}{\partial t_{J_{ot}+j}} \right]_{t=N} + \left[\frac{\partial L(\boldsymbol{\alpha})}{\partial s_{J_{os}+j}} \right]_{s=N} + \left[\frac{\partial L(\boldsymbol{\alpha})}{\partial f_{J_{of}+J_v+j}} \right]_{f=N} + \left[\frac{\partial L(\boldsymbol{\alpha})}{\partial q_{J_q+j}} \right]_{q=N}, \quad j = 1, \dots, J_n. \quad (7)$$

The contributions arising from the macroscopic total cross sections are computed using the following particular form of Equation (150) derived in [7]:

$$\left[\frac{\partial L(\boldsymbol{\alpha})}{\partial n_j} \right]^{(1)} = \left[\frac{\partial L(\boldsymbol{\alpha})}{\partial t_{J_{ot}+j}} \right]_{t=N} = - \sum_{g=1}^G \int dV \int_{4\pi} d\boldsymbol{\Omega} \psi^{(1),g}(r, \boldsymbol{\Omega}) \varphi^g(r, \boldsymbol{\Omega}) \frac{\partial \Sigma_t^g(\mathbf{t})}{\partial n_j}, \quad j = 1, \dots, J_n. \quad (8)$$

The multigroup adjoint fluxes $\psi^{(1),g}(r, \boldsymbol{\Omega})$, $g = 1, \dots, G$, appearing in Equation (8) are the solutions of the following 1st-Level Adjoint Sensitivity System (1st-LASS) presented in Equations (156) and (157) of [7]:

$$A^{(1),g}(\boldsymbol{\alpha}) \psi^{(1),g}(r, \boldsymbol{\Omega}) = \boldsymbol{\Omega} \cdot \mathbf{n} \delta(r - r_d), \quad g = 1, \dots, G, \quad (9)$$

$$\psi^{(1),g}(r_d, \boldsymbol{\Omega}) = 0, \quad \boldsymbol{\Omega} \cdot \mathbf{n} > 0, \quad g = 1, \dots, G, \quad (10)$$

where the adjoint operator $A^{(1),g}(\boldsymbol{\alpha})$ takes on the following particular form of Equation (149) in [7]:

$$\begin{aligned} & A^{(1),g}(\boldsymbol{\alpha}) \psi^{(1),g}(r, \boldsymbol{\Omega}) \\ & \triangleq -\boldsymbol{\Omega} \cdot \nabla \psi^{(1),g}(r, \boldsymbol{\Omega}) + \Sigma_t^g(\mathbf{t}) \psi^{(1),g}(r, \boldsymbol{\Omega}) - \sum_{g'=14\pi}^G \int d\boldsymbol{\Omega}' \Sigma_s^{g \rightarrow g'}(\mathbf{s}; \boldsymbol{\Omega} \rightarrow \boldsymbol{\Omega}') \psi^{(1),g'}(r, \boldsymbol{\Omega}') \\ & - \nu \Sigma_f^g(\mathbf{f}) \sum_{g'=14\pi}^G \int d\boldsymbol{\Omega}' \chi^{g'} \psi^{(1),g'}(r, \boldsymbol{\Omega}'), \quad g = 1, \dots, G. \end{aligned} \quad (11)$$

For the PERP benchmark, the parameter n_j , $j = 1, \dots, J_n$ corresponds to the isotopic number density, i.e., $n_j \equiv N_{i_j, m_j}$, where the subscripts i_j and m_j denote, respectively, the isotope and material associated with the parameter n_j . Hence, the following relation holds:

$$\frac{\partial \Sigma_t^g(\mathbf{t})}{\partial n_j} = \frac{\partial \Sigma_t^g(\mathbf{t})}{\partial N_{i_j, m_j}} = \frac{\partial \left[\sum_{m=1}^M \sum_{i=1}^I N_{i, m} \sigma_{t, i}^g \right]}{\partial N_{i_j, m_j}} = \sigma_{t, i_j}^g. \quad (12)$$

Inserting Equation (12) into Equation (8) yields:

$$\left[\frac{\partial L(\boldsymbol{\alpha})}{\partial n_j} \right]^{(1)} = \left[\frac{\partial L(\boldsymbol{\alpha})}{\partial t_{J_{ot}+j}} \right]_{t=N} = - \sum_{g=1}^G \int dV \sigma_{t, i_j}^g \int_{4\pi} d\boldsymbol{\Omega} \psi^{(1),g}(r, \boldsymbol{\Omega}) \varphi^g(r, \boldsymbol{\Omega}), \quad j = 1, \dots, J_n. \quad (13)$$

The contributions resulting from the macroscopic scattering cross sections are computed using the following particular form of Equation (151) in [7]:

$$\left[\frac{\partial L(\alpha)}{\partial n_j} \right]^{(2)} = \left[\frac{\partial L(\alpha)}{\partial s_{j\sigma_s+j}} \right]_{s=N} = \sum_{g=1}^G \int dV \int_{4\pi} d\Omega \psi^{(1),g}(r, \Omega) \sum_{g'=1}^G \int_{4\pi} d\Omega' \frac{\partial \Sigma_s^{g' \rightarrow g}(s; \Omega' \rightarrow \Omega)}{\partial n_j} \varphi^{g'}(r, \Omega'), \quad (14)$$

for $j = 1, \dots, J_n$.

Noting that:

$$\begin{aligned} \frac{\partial \Sigma_s^{g' \rightarrow g}(s; \Omega' \rightarrow \Omega)}{\partial n_j} &= \frac{\partial \Sigma_s^{g' \rightarrow g}(s; \Omega' \rightarrow \Omega)}{\partial N_{i_j, m_j}} = \frac{\partial \left[\sum_{m=1}^M \sum_{i=1}^I N_{i, m} \sigma_{s, i}^{g' \rightarrow g}(s; \Omega' \rightarrow \Omega) \right]}{\partial N_{i_j, m_j}} \\ &= \frac{\partial \left[\sum_{m=1}^M \sum_{i=1}^I \sum_{l=0}^{ISCT} N_{i, m} (2l+1) \sigma_{s, l, i}^{g' \rightarrow g} P_l(\Omega' \cdot \Omega) \right]}{\partial N_{i_j, m_j}} = \sum_{l=0}^{ISCT} (2l+1) \sigma_{s, l, i_j}^{g' \rightarrow g} P_l(\Omega' \cdot \Omega). \end{aligned} \quad (15)$$

Inserting Equation (15) into Equation (14), using the addition theorem for spherical harmonics in one-dimensional geometry, and performing the respective angular integrations yields:

$$\left[\frac{\partial L(\alpha)}{\partial n_j} \right]^{(2)} = \left[\frac{\partial L(\alpha)}{\partial s_{j\sigma_s+j}} \right]_{s=N} = \sum_{g=1}^G \sum_{l=0}^{ISCT} (2l+1) \int dV \xi_l^{(1),g}(r) \sum_{g'=1}^G \sigma_{s, l, i_j}^{g' \rightarrow g} \varphi_l^{g'}(r), \quad j = 1, \dots, J_n, \quad (16)$$

where:

$$\varphi_l^g(r) \triangleq \int_{4\pi} d\Omega P_l(\Omega) \varphi^g(r, \Omega), \quad (17)$$

$$\xi_l^{(1),g}(r) \triangleq \int_{4\pi} d\Omega P_l(\Omega) \psi^{(1),g}(r, \Omega). \quad (18)$$

The contributions stemming from the macroscopic fission cross sections are computed using the following particular form of Equation (152) in [7]:

$$\left[\frac{\partial L(\alpha)}{\partial n_j} \right]^{(3)} = \left[\frac{\partial L(\alpha)}{\partial f_{j\sigma_f+J_v+j}} \right]_{f=N} = \sum_{g=1}^G \int_V dV \int_{4\pi} d\Omega \psi^{(1),g}(r, \Omega) \sum_{g'=1}^G \int_{4\pi} d\Omega' \frac{\partial \left[(v\Sigma_f)^{g'}(\mathbf{f}) \right]}{\partial n_j} \chi^g \varphi^{g'}(r, \Omega'), \quad (19)$$

for $j = 1, \dots, J_n$.

Inserting the result below:

$$\frac{\partial \left[(v\Sigma_f)^{g'}(\mathbf{f}) \right]}{\partial n_j} = \frac{\partial \left[(v\Sigma_f)^{g'}(\mathbf{f}) \right]}{\partial N_{i_j, m_j}} = \frac{\partial \sum_{m=1}^M \sum_{i=1}^I N_{i, m} (v\sigma_f)_i^{g'}}{\partial N_{i_j, m_j}} = \frac{\partial \sum_{m=1}^M \sum_{i=1}^I N_{i, m} v_i^{g'} \sigma_{f, i}^{g'}}{\partial N_{i_j, m_j}} = v_{i_j}^{g'} \sigma_{f, i_j}^{g'} \quad (20)$$

into Equation (19) and performing the respective angular integrations yields:

$$\left[\frac{\partial L(\alpha)}{\partial n_j} \right]^{(3)} = \left[\frac{\partial L(\alpha)}{\partial f_{j\sigma_f+J_v+j}} \right]_{f=N} = \sum_{g=1}^G \int_V dV \xi_0^{(1),g}(r) \chi^g \sum_{g'=1}^G v_{i_j}^{g'} \sigma_{f, i_j}^{g'} \varphi_0^{g'}(r), \quad j = 1, \dots, J_n, \quad (21)$$

where:

$$\varphi_0^g(r) \triangleq \int_{4\pi} d\Omega \varphi^g(r, \Omega), \quad (22)$$

$$\xi_0^{(1),g}(r) \triangleq \int_{4\pi} d\Omega \psi^{(1),g}(r, \Omega). \quad (23)$$

The contributions arising from the source are computed using the following particular form of Equation (154) in [7]:

$$\left[\frac{\partial L(\alpha)}{\partial n_j} \right]^{(4)} = \left[\frac{\partial L(\alpha)}{\partial q_{J_q+j}} \right]_{q=N} = \sum_{g=1}^G \int_V dV \int_{4\pi} d\Omega \psi^{(1),g}(r, \Omega) \frac{\partial Q^g(\mathbf{q}; r, \Omega)}{\partial n_j}, \quad j = 1, \dots, J_n, \quad (24)$$

where the source Q^g is the sum of all sources of neutrons in in group g . Since the PERP benchmark contains just spontaneous fission sources, it follows that:

$$Q^g = Q_{SF}^g, \quad (25)$$

where Q_{SF}^g denotes the total spontaneous fission source rate density in group g . The spontaneous fission source rate density $Q_{SF,k}^g$ in group g for isotope k for the PERP benchmark is modeled by the following expression:

$$Q_{SF,k}^g = \lambda_k N_{k,m} \chi_{SF,k}^g = \lambda_k N_{k,m} F_k^{SF} \mathbf{v}_k^{SF} \left(\frac{2}{\sqrt{\pi a_k^3 b_k}} e^{-\frac{a_k b_k}{4}} \right) \int_{E_{s+1}}^{E^g} dE e^{-E/a_k} \sinh \sqrt{b_k E}, \quad (26)$$

where λ_k is the decay constant for isotope k , and $\chi_{SF,k}^g$ includes the spontaneous fission branch ratio and the spontaneous fission neutron spectra, which are approximated by a Watt's fission spectrum using two evaluated parameters (a_k and b_k). The total spontaneous fission source rate density in group g , Q_{SF}^g , is the sum over all fissionable isotopes, i.e.:

$$Q_{SF}^g = \sum_{m=1}^M \sum_{k=1}^{N_f} Q_{SF,k}^g = \sum_{m=1}^M \sum_{k=1}^{N_f} \lambda_k N_{k,m} \chi_{SF,k}^g. \quad (27)$$

Since:

$$\frac{\partial Q^g(\mathbf{q}; r, \Omega)}{\partial n_j} = \frac{\partial Q_{SF}^g}{\partial N_{i_j, m_j}} = \frac{\partial \sum_{m=1}^M \sum_{k=1}^{N_f} \lambda_k N_{k,m} \chi_{SF,k}^g}{\partial N_{i_j, m_j}} = \lambda_{i_j} \chi_{SF, i_j}^g = \frac{Q_{SF, i_j}^g}{N_{i_j, m_j}} = \frac{Q_{SF, i_j}^g}{n_j}, \quad (28)$$

the last term on the right side of Equation (28) is inserted into Equation (24), which enables performing the respective angular integrations to obtain:

$$\left[\frac{\partial L(\alpha)}{\partial n_j} \right]^{(4)} = \left[\frac{\partial L(\alpha)}{\partial q_{J_q+j}} \right]_{q=N} = \frac{1}{n_j} \sum_{g=1}^G \int_V dV \xi_0^{(1),g}(r) Q_{SF, i_j}^g, \quad j = 1, \dots, J_n. \quad (29)$$

Adding the partial contributions from Equations (13), (16), (21) and (29) yields the following complete expression for $\partial L(\alpha) / \partial n_j$ in terms of the isotopic number density parameter $n_j \equiv N_{i_j, m_j}$:

$$\begin{aligned} \frac{\partial L(\alpha)}{\partial n_j} &= \sum_{i=1}^4 \left[\frac{\partial L(\alpha)}{\partial n_j} \right]^{(i)} \\ &= - \sum_{g=1}^G \int dV \sigma_{t, i_j}^g \int_{4\pi} d\Omega \psi^{(1),g}(r, \Omega) \varphi^g(r, \Omega) + \sum_{g=1}^G \sum_{l=0}^{ISCT} (2l+1) \int dV \xi_l^{(1),g}(r) \sum_{g'=1}^G \sigma_{s, l, i_j}^{g' \rightarrow g} \varphi_l^{g'}(r) \\ &+ \sum_{g=1}^G \int_V dV \xi_0^{(1),g}(r) \chi^g \sum_{g'=1}^G \mathbf{v}_j^{g'} \sigma_{f, i_j}^{g'} \varphi_0^{g'}(r) + \frac{1}{n_j} \sum_{g=1}^G \int_V dV \xi_0^{(1),g}(r) Q_{SF, i_j}^g, \text{ for } j = 1, \dots, J_n. \end{aligned} \quad (30)$$

The 1st-order relative sensitivities corresponding to $\partial L(\alpha) / \partial n_j$ are defined as $S^{(1)}(N_{i,m}) \triangleq (\partial L / \partial N_{j,m})(N_{j,m} / L)$, $i = 1, \dots, I; m = 1, \dots, M$. The numerical values of the 1st-order relative sensitivities $S^{(1)}(N_{i,m})$ of leakage response with respect to the isotope number densities for the six isotopes contained in the PERP benchmark will be presented in Section 3, below, in the table that comparing these values with the numerical values of the corresponding 2nd-order unmixed relative sensitivities $S^{(2)}(N_{i,m}, N_{i,m}) \triangleq (\partial^2 L / \partial N_{i,m} \partial N_{i,m})(N_{i,m} N_{i,m} / L)$, $j = 1, \dots, I; m = 1, \dots, M$.

3. Computation of the 2nd-Order Mixed and Unmixed Sensitivities of the PERP Leakage Response with Respect to the Isotopic Number Densities

The complete expression of the 2nd-order sensitivities $\partial^2 L(\alpha) / \partial N \partial N$ comprises 16 components, which stem from the neutron sources and from the total, scattering and fission macroscopic cross sections. The expression of $\partial^2 L(\alpha) / \partial N \partial N$ is as follows:

$$\begin{aligned} \frac{\partial^2 L}{\partial n_j \partial n_{m_2}} = & \left[\frac{\partial^2 L}{\partial t_{lot+j} \partial t_{lot+m_2}} \right]_{t=N, t=N} + \left[\frac{\partial^2 L}{\partial t_{lot+j} \partial s_{los+m_2}} \right]_{t=N, s=N} + \left[\frac{\partial^2 L}{\partial t_{lot+j} \partial f_{lof+l_v+m_2}} \right]_{t=N, f=N} \\ & + \left[\frac{\partial^2 L}{\partial t_{lot+j} \partial q_{lq+m_2}} \right]_{t=N, q=N} + \left[\frac{\partial^2 L}{\partial s_{los+j} \partial t_{lot+m_2}} \right]_{s=N, t=N} + \left[\frac{\partial^2 L}{\partial s_{los+j} \partial s_{los+m_2}} \right]_{s=N, s=N} \\ & + \left[\frac{\partial^2 L}{\partial s_{los+j} \partial f_{lof+l_v+m_2}} \right]_{s=N, f=N} + \left[\frac{\partial^2 L}{\partial s_{los+j} \partial q_{lq+m_2}} \right]_{s=N, q=N} + \left[\frac{\partial^2 L}{\partial f_{lof+l_v+j} \partial t_{lot+m_2}} \right]_{f=N, t=N} \\ & + \left[\frac{\partial^2 L}{\partial f_{lof+l_v+j} \partial s_{los+m_2}} \right]_{f=N, s=N} + \left[\frac{\partial^2 L}{\partial f_{lof+l_v+j} \partial f_{lof+l_v+m_2}} \right]_{f=N, f=N} + \left[\frac{\partial^2 L}{\partial f_{lof+l_v+j} \partial q_{lq+m_2}} \right]_{f=N, q=N} \\ & + \left[\frac{\partial^2 L}{\partial q_{lq+j} \partial t_{lot+m_2}} \right]_{q=N, t=N} + \left[\frac{\partial^2 L}{\partial q_{lq+j} \partial s_{los+m_2}} \right]_{q=N, s=N} + \left[\frac{\partial^2 L}{\partial q_{lq+j} \partial f_{lof+l_v+m_2}} \right]_{q=N, f=N} \\ & + \left[\frac{\partial^2 L}{\partial q_{lq+j} \partial q_{lq+m_2}} \right]_{q=N, q=N}, \text{ for } j = 1, \dots, J_n; m_2 = 1, \dots, J_n. \end{aligned} \quad (31)$$

The 16 components shown on the right-side of Equation (31) are obtained by particularizing Equations (158), (159), (160), (162), (167), (168), (169), (171), (177), (178), (179), (181), (204), (205), (206) and (208) in [7] to the PERP benchmark. Thus, the contribution stemming from the macroscopic total cross sections is obtained by particularizing Equation (158) in [7] to the PERP benchmark, to obtain:

$$\begin{aligned} \left(\frac{\partial^2 L}{\partial n_j \partial n_{m_2}} \right)^{(1)} = & \left[\frac{\partial^2 L}{\partial t_{lot+j} \partial t_{lot+m_2}} \right]_{t=N, t=N} = - \sum_{g=1}^G \int_V dV \int_{4\pi} d\Omega \psi^{(1),g}(r, \Omega) \varphi^g(r, \Omega) \frac{\partial^2 \Sigma_t^g(\mathbf{t})}{\partial n_j \partial n_{m_2}} \\ & - \sum_{g=1}^G \int_V dV \int_{4\pi} d\Omega \left[\psi_{1,i}^{(2),g}(r, \Omega) \psi^{(1),g}(r, \Omega) + \psi_{2,i}^{(2),g}(r, \Omega) \varphi^g(r, \Omega) \right] \frac{\partial \Sigma_t^g(\mathbf{t})}{\partial n_{m_2}}, \end{aligned} \quad (32)$$

for $j = 1, \dots, J_n; m_2 = 1, \dots, J_n$.

The 2nd-level adjoint functions $\psi_{1,i}^{(2),g}$ and $\psi_{2,i}^{(2),g}, j = 1, \dots, J_n; g = 1, \dots, G$, in Equation (32) are the solutions of the following 2nd-Level Adjoint Sensitivity System (2nd-LASS) presented in Equations (164)–(166) of [7]:

$$B^g(\alpha^0) \psi_{1,i}^{(2),g}(r, \Omega) = -\varphi^g(r, \Omega) \frac{\partial \Sigma_t^g(\mathbf{t})}{\partial n_i}, \quad i = 1, \dots, J_n; g = 1, \dots, G, \quad (33)$$

$$\psi_{1,i}^{(2),g}(r_d, \Omega) = 0, \quad \Omega \cdot \mathbf{n} < 0; \quad i = 1, \dots, J_n; g = 1, \dots, G, \quad (34)$$

$$A^{(1),g}(\alpha^0) \psi_{2,i}^{(2),g}(r, \Omega) = -\psi^{(1),g}(r, \Omega) \frac{\partial \Sigma_t^g(\mathbf{t})}{\partial n_j}, \quad i = 1, \dots, J_n; g = 1, \dots, G, \quad (35)$$

$$\psi_{2,i}^{(2),g}(r_d, \Omega) = 0, \quad \Omega \cdot \mathbf{n} > 0; \quad i = 1, \dots, J_n; g = 1, \dots, G. \quad (36)$$

The parameters $n_j, j = 1, \dots, J_n$ and $n_{m_2}, m_2 = 1, \dots, J_n$ which appear in Equation (32) correspond to the following isotopic number densities: $n_j \equiv N_{i_j, m_j}$ and $n_{m_2} \equiv N_{i_{m_2}, m_{m_2}}$, respectively; the subscripts i_{m_2} and m_{m_2} denote the isotope and material associated with the parameter n_{m_2} . Consequently, the following results hold:

$$\frac{\partial^2 \Sigma_t^g(\mathbf{t})}{\partial n_j \partial n_{m_2}} = \frac{\partial^2 \Sigma_t^g(\mathbf{t})}{\partial N_{i_j, m_j} \partial N_{i_{m_2}, m_{m_2}}} = 0, \quad (37)$$

$$\frac{\partial \Sigma_t^g(\mathbf{t})}{\partial n_{m_2}} = \frac{\partial \Sigma_t^g(\mathbf{t})}{\partial N_{i_{m_2}, m_{m_2}}} = \frac{\partial \left(\sum_{m=1}^M \sum_{i=1}^I N_{i, m} \sigma_{t, i}^g \right)}{\partial N_{i_{m_2}, m_{m_2}}} = \sigma_{t, i_{m_2}}^g, \quad (38)$$

$$\frac{\partial \Sigma_{t^g}(\mathbf{t})}{\partial n_j} = \frac{\partial \Sigma_{t^g}(\mathbf{t})}{\partial N_{i_j, m_j}} = \frac{\partial \left(\sum_{m=1}^M \sum_{i=1}^I N_{i, m} \sigma_{t, i}^g \right)}{\partial N_{i_j, m_j}} = \sigma_{t, i_j}^g. \tag{39}$$

Inserting Equations (37)–(39) into Equation (32) yields:

$$\left(\frac{\partial^2 L}{\partial n_j \partial n_{m_2}} \right)^{(1)} = - \sum_{g=1}^G \int_V dV \int_{4\pi} d\Omega \left[\psi_{1, j}^{(2), g}(r, \Omega) \psi^{(1), g}(r, \Omega) + \psi_{2, j}^{(2), g}(r, \Omega) \varphi^g(r, \Omega) \right] \sigma_{t, i_{m_2}}^g, \tag{40}$$

for $j = 1, \dots, J_n; m_2 = 1, \dots, J_n$,

where the 2nd-level adjoint functions $\psi_{1, j}^{(2), g}$, and $\psi_{2, j}^{(2), g}$, $j = 1, \dots, J_n; g = 1, \dots, G$, are the solutions of the following particular forms of Equations (33) and (35):

$$B^g(\alpha^0) \psi_{1, j}^{(2), g}(r, \Omega) = -\sigma_{t, i_j}^g \varphi^g(r, \Omega), \quad j = 1, \dots, J_n; \quad g = 1, \dots, G, \tag{41}$$

$$A^{(1), g}(\alpha^0) \psi_{2, j}^{(2), g}(r, \Omega) = -\sigma_{t, i_j}^g \psi^{(1), g}(r, \Omega), \quad j = 1, \dots, J_n; \quad g = 1, \dots, G, \tag{42}$$

while being subject to the boundary conditions shown in Equations (34) and (36).

The contribution stemming from the macroscopic total and scattering cross sections is obtained by particularizing Equation (159) in [7] to the PERP benchmark, which yields:

$$\begin{aligned} \left(\frac{\partial^2 L}{\partial n_j \partial n_{m_2}} \right)^{(2)} &= \left[\frac{\partial^2 L}{\partial t_{i_{ot}+j} \partial s_{ios+m_2}} \right]_{t=N, s=N} \\ &= \sum_{g=1}^G \int_V dV \int_{4\pi} d\Omega \psi_{1, j}^{(2), g}(r, \Omega) \sum_{g'=1}^G \int_{4\pi} d\Omega' \psi^{(1), g'}(r, \Omega') \frac{\partial \Sigma_s^{g \rightarrow g'}(\mathbf{s}; \Omega \rightarrow \Omega')}{\partial n_{m_2}} \\ &+ \sum_{g=1}^G \int_V dV \int_{4\pi} d\Omega \psi_{2, j}^{(2), g}(r, \Omega) \sum_{g'=1}^G \int_{4\pi} d\Omega' \varphi^{g'}(r, \Omega') \frac{\partial \Sigma_s^{g' \rightarrow g}(\mathbf{s}; \Omega' \rightarrow \Omega)}{\partial n_{m_2}}, \end{aligned} \tag{43}$$

for $j = 1, \dots, J_n; m_2 = 1, \dots, J_n$.

Note the following relations:

$$\frac{\partial \Sigma_s^{g \rightarrow g'}(\mathbf{s}; \Omega \rightarrow \Omega')}{\partial n_{m_2}} = \frac{\partial \Sigma_s^{g \rightarrow g'}(\mathbf{s}; \Omega \rightarrow \Omega')}{\partial N_{i_{m_2}, m_{m_2}}} = \sum_{l=0}^{ISCT} (2l+1) \sigma_{s, l, i_{m_2}}^{g \rightarrow g'} P_l(\Omega' \cdot \Omega), \tag{44}$$

$$\frac{\partial \Sigma_s^{g' \rightarrow g}(\mathbf{s}; \Omega' \rightarrow \Omega)}{\partial n_{m_2}} = \frac{\partial \Sigma_s^{g' \rightarrow g}(\mathbf{s}; \Omega' \rightarrow \Omega)}{\partial N_{i_{m_2}, m_{m_2}}} = \sum_{l=0}^{ISCT} (2l+1) \sigma_{s, l, i_{m_2}}^{g' \rightarrow g} P_l(\Omega' \cdot \Omega). \tag{45}$$

Inserting the results obtained in Equations (44) and (45) into Equation (43) and performing the respective angular integrations yields the following expression for Equation (43):

$$\begin{aligned} \left(\frac{\partial^2 L}{\partial n_j \partial n_{m_2}} \right)^{(2)} &= \sum_{g=1}^G \sum_{l=0}^{ISCT} (2l+1) \int_V dV \xi_{1, j, l}^{(2), g}(r) \sum_{g'=1}^G \sigma_{s, l, i_{m_2}}^{g \rightarrow g'} \xi_l^{(1), g'}(r) \\ &+ \sum_{g=1}^G \sum_{l=0}^{ISCT} (2l+1) \int_V dV \xi_{2, j, l}^{(2), g}(r) \sum_{g'=1}^G \sigma_{s, l, i_{m_2}}^{g' \rightarrow g} \varphi_l^{g'}(r), \end{aligned} \tag{46}$$

for $j = 1, \dots, J_n; m_2 = 1, \dots, J_n$,

where:

$$\xi_{1, j, l}^{(2), g}(r) \triangleq \int_{4\pi} d\Omega P_l(\Omega) \psi_{1, j}^{(2), g}(r, \Omega), \tag{47}$$

$$\xi_{2, j, l}^{(2), g}(r) \triangleq \int_{4\pi} d\Omega P_l(\Omega) \psi_{2, j}^{(2), g}(r, \Omega). \tag{48}$$

The contribution stemming from the macroscopic total and fission cross sections is obtained by particularizing Equation (160) in [7] to the PERP benchmark, which yields:

$$\begin{aligned} \left(\frac{\partial^2 L}{\partial n_j \partial n_{m_2}}\right)^{(3)} &= \left[\frac{\partial^2 L}{\partial t_{l_{ot}+j} \partial f_{l_{of}+l_{v}+m_2}}\right]_{t=N, f=N} \\ &= \sum_{g=1}^G \int_V dV \int_{4\pi} d\Omega \psi_{2,j}^{(2),g}(r, \Omega) \sum_{g'=1}^G \int_{4\pi} d\Omega' \varphi^{g'}(r, \Omega') \chi^g \frac{\partial[(v\Sigma_f)^{g'}(\mathbf{f})]}{\partial n_{m_2}} \\ &+ \sum_{g=1}^G \int_V dV \int_{4\pi} d\Omega \psi_{1,j}^{(2),g}(r, \Omega) \frac{\partial[(v\Sigma_f)^g(\mathbf{f})]}{\partial n_{m_2}} \sum_{g'=1}^G \int_{4\pi} d\Omega' \chi^{g'} \psi^{(1),g'}(r, \Omega'), \end{aligned} \tag{49}$$

for $j = 1, \dots, J_n; m_2 = 1, \dots, J_n$.

Note that:

$$\frac{\partial(v\Sigma_f)^g(\mathbf{f})}{\partial n_{m_2}} = \frac{\partial \sum_{m=1}^M \sum_{i=1}^I N_{i,m} (v\sigma_f)_i^g}{\partial N_{i_{m_2}, m_{m_2}}} = \frac{\partial \sum_{m=1}^M \sum_{i=1}^I N_{i,m} v_i^g \sigma_{f,i}^g}{\partial N_{i_{m_2}, m_{m_2}}} = v_{i_{m_2}}^g \sigma_{f,i_{m_2}}^g, \tag{50}$$

$$\frac{\partial(v\Sigma_f)^{g'}(\mathbf{f})}{\partial n_{m_2}} = \frac{\partial \sum_{m=1}^M \sum_{i=1}^I N_{i,m} (v\sigma_f)_i^{g'}}{\partial N_{i_{m_2}, m_{m_2}}} = \frac{\partial \sum_{m=1}^M \sum_{i=1}^I N_{i,m} v_i^{g'} \sigma_{f,i}^{g'}}{\partial N_{i_{m_2}, m_{m_2}}} = v_{i_{m_2}}^{g'} \sigma_{f,i_{m_2}}^{g'}. \tag{51}$$

Inserting Equations (50) and (51) into Equation (49) and performing the respective angular integrations yields the following expression for Equation (49):

$$\begin{aligned} \left(\frac{\partial^2 L}{\partial n_j \partial n_{m_2}}\right)^{(3)} &= \sum_{g=1}^G \int_V dV \chi^g \xi_{2,j;0}^{(2),g}(r) \sum_{g'=1}^G v_{i_{m_2}}^{g'} \sigma_{f,i_{m_2}}^{g'} \varphi_0^{g'}(r) + \sum_{g=1}^G \int_V dV v_{i_{m_2}}^g \sigma_{f,i_{m_2}}^g \xi_{1,j;0}^{(2),g}(r) \sum_{g'=1}^G \chi^{g'} \xi_0^{(1),g'}(r), \end{aligned} \tag{52}$$

for $j = 1, \dots, J_n; m_2 = 1, \dots, J_n$,

where:

$$\xi_{1,j;0}^{(2),g}(r) \triangleq \int_{4\pi} d\Omega \psi_{1,j}^{(2),g}(r, \Omega), \tag{53}$$

$$\xi_{2,j;0}^{(2),g}(r) \triangleq \int_{4\pi} d\Omega \psi_{2,j}^{(2),g}(r, \Omega). \tag{54}$$

The contribution stemming from the macroscopic total cross sections and the source term is obtained by particularizing Equation (162) in [7] to the PERP benchmark, which yields:

$$\begin{aligned} \left(\frac{\partial^2 L}{\partial n_j \partial n_{m_2}}\right)^{(4)} &= \left[\frac{\partial^2 L}{\partial t_{l_{ot}+j} \partial q_{l_{q}+m_2}}\right]_{t=N, q=N} = \sum_{g=1}^G \int_V dV \int_{4\pi} d\Omega \psi_{2,j}^{(2),g}(r, \Omega) \frac{\partial Q^g(\mathbf{q}; r, \Omega)}{\partial n_{m_2}}, \end{aligned} \tag{55}$$

for $j = 1, \dots, J_n; m_2 = 1, \dots, J_n$.

Note that:

$$\frac{\partial Q^g(\mathbf{q}; r, \Omega)}{\partial n_{m_2}} = \frac{\partial Q_{SF}^g}{\partial n_{m_2}} = \frac{\partial \sum_{m=1}^M \sum_{k=1}^{N_f} \lambda_k N_{k,m} \chi_{SF,k}^g}{\partial N_{i_{m_2}, m_{m_2}}} = \lambda_{m_2} \chi_{SF,i_{m_2}}^g = \frac{Q_{SF,i_{m_2}}^g}{N_{i_{m_2}, m_{m_2}}} = \frac{Q_{SF,i_{m_2}}^g}{n_{m_2}}. \tag{56}$$

Inserting Equation (56) into Equation (55), yields the following simplified expression for Equation (55):

$$\left(\frac{\partial^2 L}{\partial n_j \partial n_{m_2}}\right)^{(4)} = \frac{1}{n_{m_2}} \sum_{g=1}^G \int_V dV \xi_{2,j;0}^{(2),g}(r) Q_{SF,i_{m_2}}^g, \quad j = 1, \dots, J_n; m_2 = 1, \dots, J_n. \tag{57}$$

The contribution stemming from the macroscopic scattering and total cross sections is obtained by particularizing Equation (167) in [7] to the PERP benchmark, which yields:

$$\begin{aligned} \left(\frac{\partial^2 L}{\partial n_j \partial n_{m_2}}\right)^{(5)} &= \left[\frac{\partial^2 L}{\partial s_{los+j} \partial t_{lot+m_2}}\right]_{s=N, t=N} \\ &= - \sum_{g=1}^G \int_V dV \int_{4\pi} d\Omega \left[\theta_{1,j}^{(2),g}(r, \Omega) \psi^{(1),g}(r, \Omega) + \theta_{2,j}^{(2),g}(r, \Omega) \varphi^g(r, \Omega) \right] \frac{\partial \Sigma_r^g(\mathbf{t})}{\partial n_{m_2}}, \\ &\text{for } j = 1, \dots, J_n; m_2 = 1, \dots, J_n, \end{aligned} \tag{58}$$

where the 2nd-level adjoint functions $\theta_{1,j}^{(2),g}$, and $\theta_{2,j}^{(2),g}$, $j = 1, \dots, J_n$; $g = 1, \dots, G$, are the solutions of the following 2nd-Level Adjoint Sensitivity System presented in Equations (164)–(166) of [7]:

$$B^g(\alpha^0) \theta_{1,j}^{(2),g}(r, \Omega) = \sum_{g'=1}^G \int_{4\pi} d\Omega' \frac{\partial \Sigma_s^{g' \rightarrow g}(\mathbf{s}; \Omega' \rightarrow \Omega)}{\partial n_j} \varphi^{g'}(r, \Omega'), j = 1, \dots, J_n; g = 1, \dots, G, \tag{59}$$

$$\theta_{1,j}^{(2),g}(r_d, \Omega) = 0, \Omega \cdot \mathbf{n} < 0; j = 1, \dots, J_n; g = 1, \dots, G, \tag{60}$$

$$A^{(1),g}(\alpha^0) \theta_{2,j}^{(2),g}(r, \Omega) = \sum_{g'=1}^G \int_{4\pi} d\Omega' \psi^{(1),g'}(r, \Omega') \frac{\partial \Sigma_s^{g \rightarrow g'}(\mathbf{s}; \Omega \rightarrow \Omega')}{\partial n_j}, j = 1, \dots, J_n; g = 1, \dots, G, \tag{61}$$

$$\theta_{2,j}^{(2),g}(r_d, \Omega) = 0, \Omega \cdot \mathbf{n} > 0; j = 1, \dots, J_n; g = 1, \dots, G. \tag{62}$$

For the PERP benchmark, the following relation holds:

$$\frac{\partial \Sigma_s^{g \rightarrow g'}(\mathbf{s}; \Omega \rightarrow \Omega')}{\partial n_j} = \frac{\partial \Sigma_s^{g \rightarrow g'}(\mathbf{s}; \Omega \rightarrow \Omega')}{\partial N_{i_j, m_j}} = \sum_{l=0}^{ISCT} (2l+1) \sigma_{s,l,i_j}^{g \rightarrow g'} P_l(\Omega' \cdot \Omega). \tag{63}$$

Inserting Equations (15), (38) and (63) into Equations (59), (61) and (58) reduces the latter equation to the following expression:

$$\begin{aligned} \left(\frac{\partial^2 L}{\partial n_j \partial n_{m_2}}\right)^{(5)} &= - \sum_{g=1}^G \int_V dV \sigma_{t,i,m_2}^g \int_{4\pi} d\Omega \left[\theta_{1,j}^{(2),g}(r, \Omega) \psi^{(1),g}(r, \Omega) + \theta_{2,j}^{(2),g}(r, \Omega) \varphi^g(r, \Omega) \right], \\ &\text{for } j = 1, \dots, J_n; m_2 = 1, \dots, J_n, \end{aligned} \tag{64}$$

where the 2nd-level adjoint functions $\theta_{1,j}^{(2),g}$, and $\theta_{2,j}^{(2),g}$, $j = 1, \dots, J_n$; $g = 1, \dots, G$, are the solutions of the following particular forms of Equations (59) and (61):

$$B^g(\alpha^0) \theta_{1,j}^{(2),g}(r, \Omega) = \sum_{g'=1}^G \sum_{l=0}^{ISCT} (2l+1) \sigma_{s,l,i_j}^{g' \rightarrow g} P_l(\Omega) \phi_l^{g'}(r), j = 1, \dots, J_n; g = 1, \dots, G, \tag{65}$$

$$A^{(1),g}(\alpha^0) \theta_{2,j}^{(2),g}(r, \Omega) = \sum_{g'=1}^G \sum_{l=0}^{ISCT} (2l+1) \sigma_{s,l,i_j}^{g \rightarrow g'} P_l(\Omega) \xi_l^{(1),g'}(r), j = 1, \dots, J_n; g = 1, \dots, G, \tag{66}$$

while being subject to the boundary conditions shown in Equations (60) and (62). Due to symmetry, the result obtained in Equation (64) for $\left(\frac{\partial^2 L}{\partial n_j \partial n_{m_2}}\right)^{(5)} = \left[\frac{\partial^2 L}{\partial s_{los+j} \partial t_{lot+m_2}}\right]_{s=N, t=N}$ must equal to the result obtained in Equation (46) for $\left(\frac{\partial^2 L}{\partial n_j \partial n_{m_2}}\right)^{(2)} = \left[\frac{\partial^2 L}{\partial t_{lot+j} \partial s_{los+m_2}}\right]_{t=N, s=N}$.

The contribution stemming from the macroscopic scattering cross sections is obtained by particularizing Equation (168) in [7] to the PERP benchmark, which yields:

$$\begin{aligned} \left(\frac{\partial^2 L}{\partial n_j \partial n_{m_2}}\right)^{(6)} &= \left[\frac{\partial^2 L}{\partial s_{Ios+j} \partial s_{Ios+j}}\right]_{s=N, s=N} \\ &= \sum_{g=1}^G \int_V dV \int_{4\pi} d\Omega \psi^{(1),g}(r, \Omega) \sum_{g'=1}^G \int_{4\pi} d\Omega' \varphi^{g'}(r, \Omega') \frac{\partial^2 \Sigma_s^{g' \rightarrow g}(\mathbf{s}; \Omega' \rightarrow \Omega)}{\partial n_j \partial n_{m_2}} \\ &+ \sum_{g=1}^G \int_V dV \int_{4\pi} d\Omega \theta_{1,j}^{(2),g}(r, \Omega) \sum_{g'=1}^G \int_{4\pi} d\Omega' \psi^{(1),g'}(r, \Omega') \frac{\partial \Sigma_s^{g \rightarrow g'}(\mathbf{s}; \Omega \rightarrow \Omega')}{\partial n_{m_2}} \\ &+ \sum_{g=1}^G \int_V dV \int_{4\pi} d\Omega \theta_{2,j}^{(2),g}(r, \Omega) \sum_{g'=1}^G \int_{4\pi} d\Omega' \varphi^{g'}(r, \Omega') \frac{\partial \Sigma_s^{g' \rightarrow g}(\mathbf{s}; \Omega' \rightarrow \Omega)}{\partial n_{m_2}}, \end{aligned} \tag{67}$$

for $j = 1, \dots, J_n; m_2 = 1, \dots, J_n$.

Noting that:

$$\frac{\partial^2 \Sigma_s^{g' \rightarrow g}(\mathbf{s}; \Omega' \rightarrow \Omega)}{\partial n_j \partial n_{m_2}} = 0, \tag{68}$$

and inserting Equations (44) and (45) into Equation (67) yields the following expression for the latter equation:

$$\begin{aligned} \left(\frac{\partial^2 L}{\partial n_j \partial n_{m_2}}\right)^{(6)} &= \sum_{g=1}^G \sum_{l=0}^{ISCT} (2l+1) \int_V dV \Theta_{1,j,l}^{(2),g}(r) \sum_{g'=1}^G \sigma_{s,l,m_2}^{g \rightarrow g'} \xi_l^{(1),g'}(r) + \sum_{g=1}^G \sum_{l=0}^{ISCT} (2l+1) \int_V dV \Theta_{2,j,l}^{(2),g}(r) \sum_{g'=1}^G \sigma_{s,l,m_2}^{g' \rightarrow g} \varphi_l^{g'}(r), \\ &\text{for } j = 1, \dots, J_n; m_2 = 1, \dots, J_n, \end{aligned} \tag{69}$$

where:

$$\Theta_{1,j,l}^{(2),g}(r) \triangleq \int_{4\pi} d\Omega P_l(\Omega) \theta_{1,j}^{(2),g}(r, \Omega), \tag{70}$$

$$\Theta_{2,j,l}^{(2),g}(r) \triangleq \int_{4\pi} d\Omega P_l(\Omega) \theta_{2,j}^{(2),g}(r, \Omega). \tag{71}$$

The contribution stemming from the macroscopic scattering and fission cross sections is obtained by particularizing Equation (169) in [7] to the PERP benchmark, which yields:

$$\begin{aligned} \left(\frac{\partial^2 L}{\partial n_j \partial n_{m_2}}\right)^{(7)} &= \left[\frac{\partial^2 L}{\partial s_{Ios+j} \partial f_{Iof+Iv+m_2}}\right]_{s=N, f=N} \\ &= \sum_{g=1}^G \int_V dV \int_{4\pi} d\Omega \theta_{1,j}^{(2),g}(r, \Omega) \frac{\partial [(v\Sigma_f)^g(\mathbf{f})]}{\partial n_{m_2}} \sum_{g'=1}^G \int_{4\pi} d\Omega' \chi^{g'} \psi^{(1),g'}(r, \Omega') \\ &+ \sum_{g=1}^G \int_V dV \int_{4\pi} d\Omega \theta_{2,j}^{(2),g}(r, \Omega) \sum_{g'=1}^G \int_{4\pi} d\Omega' \varphi^{g'}(r, \Omega') \chi^g \frac{\partial [(v\Sigma_f)^{g'}(\mathbf{f})]}{\partial n_{m_2}}, \end{aligned} \tag{72}$$

for $j = 1, \dots, J_n; m_2 = 1, \dots, J_n$.

Inserting Equations (50) and (51) into Equation (72) yields the following expression for the latter equation:

$$\begin{aligned} \left(\frac{\partial^2 L}{\partial n_j \partial n_{m_2}}\right)^{(7)} &= \sum_{g=1}^G \int_V dV v_{im_2}^g \sigma_{f,im_2}^g \Theta_{1,j,0}^{(2),g}(r) \sum_{g'=1}^G \chi^{g'} \xi_0^{(1),g'}(r) + \sum_{g=1}^G \int_V dV \chi^g \Theta_{2,j,0}^{(2),g}(r) \sum_{g'=1}^G v_{im_2}^{g'} \sigma_{f,im_2}^{g'} \varphi_0^{g'}(r), \\ &\text{for } j = 1, \dots, J_n; m_2 = 1, \dots, J_n. \end{aligned} \tag{73}$$

where:

$$\Theta_{1,j,0}^{(2),g}(r) \triangleq \int_{4\pi} d\Omega \theta_{1,j}^{(2),g}(r, \Omega), \tag{74}$$

$$\Theta_{2,j,0}^{(2),g}(r) \triangleq \int_{4\pi} d\Omega \theta_{2,j}^{(2),g}(r, \Omega). \tag{75}$$

The contribution stemming from the macroscopic scattering cross sections and the source term is obtained by particularizing Equation (171) in [7] to the PERP benchmark, which yields:

$$\left(\frac{\partial^2 L}{\partial n_j \partial n_{m_2}}\right)^{(8)} = \left[\frac{\partial^2 L}{\partial s_{l_0 s + j} \partial q_{l_0 + m_2}} \right]_{s=N, q=N} = \sum_{g=1}^G \int_V dV \int_{4\pi} d\Omega \theta_{2,j}^{(2),g}(r, \Omega) \frac{\partial Q^g(\mathbf{q}, r, \Omega)}{\partial n_{m_2}},$$

for $j = 1, \dots, J_n; m_2 = 1, \dots, J_n$.

Inserting Equation (56) into Equation (76) yields the following expression for Equation (76):

$$\left(\frac{\partial^2 L}{\partial n_j \partial n_{m_2}}\right)^{(8)} = \frac{1}{n_{m_2}} \sum_{g=1}^G \int_V dV \Theta_{2,j;0}^{(2),g}(r) Q_{SF,im_2}^g, \quad j = 1, \dots, J_n; m_2 = 1, \dots, J_n.$$

The contribution stemming from the macroscopic fission and total cross sections is obtained by particularizing Equation (177) in [7] to the PERP benchmark, which yields:

$$\left(\frac{\partial^2 L}{\partial n_j \partial n_{m_2}}\right)^{(9)} = \left[\frac{\partial^2 L}{\partial f_{l_0 f + l_0 + j} \partial t_{l_0 t + m_2}} \right]_{f=N, t=N}$$

$$= - \sum_{g=1}^G \int_V dV \int_{4\pi} d\Omega \left[u_{1,j}^{(2),g}(r, \Omega) \psi^{(1),g}(r, \Omega) + u_{2,j}^{(2),g}(r, \Omega) \varphi^g(r, \Omega) \right] \frac{\partial \Sigma_t^g(\mathbf{t})}{\partial n_{m_2}},$$

for $j = 1, \dots, J_n; m_2 = 1, \dots, J_n$,

where the 2nd-level adjoint functions $u_{1,j}^{(2),g}$, and $u_{2,j}^{(2),g}, j = 1, \dots, J_n; g = 1, \dots, G$, are the solutions of the following 2nd-Level Adjoint Sensitivity System presented in Equations (183)–(185) of [7], namely:

$$B^g(\alpha^0) u_{1,j}^{(2),g}(r, \Omega) = \sum_{g'=1}^G \int_{4\pi} d\Omega' \varphi^{g'}(r, \Omega') \chi^{g'} \frac{\partial [(v\Sigma_f)^{g'}(\mathbf{f})]}{\partial n_j}, \quad j = 1, \dots, J_n; g = 1, \dots, G,$$

$$u_{1,j}^{(2),g}(r_d, \Omega) = 0, \quad \Omega \cdot \mathbf{n} < 0; j = 1, \dots, J_n; g = 1, \dots, G,$$

$$A^{(1),g}(\alpha^0) u_{2,j}^{(2),g}(r, \Omega) = \frac{\partial [(v\Sigma_f)^g(\mathbf{f})]}{\partial n_j} \sum_{g'=1}^G \int_{4\pi} d\Omega' \psi^{(1),g'}(r, \Omega') \chi^{g'}, \quad j = 1, \dots, J_n; g = 1, \dots, G,$$

$$u_{2,j}^{(2),g}(r_d, \Omega) = 0, \quad \Omega \cdot \mathbf{n} > 0; j = 1, \dots, J_n; g = 1, \dots, G.$$

For the PERP benchmark, the following relation holds:

$$\frac{\partial [(v\Sigma_f)^g(\mathbf{f})]}{\partial n_j} = \frac{\partial [(v\Sigma_f)^g(\mathbf{f})]}{\partial N_{i_j, m_j}} = \frac{\partial \sum_{m=1}^M \sum_{i=1}^I N_{i,m} v_i^g \sigma_{f,i}^g}{\partial N_{i_j, m_j}} = v_j^g \sigma_{f,i_j}^g.$$

Inserting Equations (20), (38) and (83) into Equations (79), (81) and (78) reduces the latter equation to the following expression:

$$\left(\frac{\partial^2 L}{\partial n_j \partial n_{m_2}}\right)^{(9)} = - \sum_{g=1}^G \int_V dV \int_{4\pi} d\Omega \left[u_{1,j}^{(2),g}(r, \Omega) \psi^{(1),g}(r, \Omega) + u_{2,j}^{(2),g}(r, \Omega) \varphi^g(r, \Omega) \right] \sigma_{t,im_2}^g,$$

for $j = 1, \dots, J_n; m_2 = 1, \dots, J_n$,

where the 2nd-level adjoint functions $u_{1,j}^{(2),g}$, and $u_{2,j}^{(2),g}, j = 1, \dots, J_n; g = 1, \dots, G$, are the solutions of the following particular forms of Equations (79) and (81):

$$B^g(\alpha^0) u_{1,j}^{(2),g}(r, \Omega) = \chi^{g'} \sum_{g'=1}^G v_{ij}^g \sigma_{f,i_j}^{g'} \varphi_0^{g'}(r), \quad j = 1, \dots, J_n; g = 1, \dots, G,$$

$$A^{(1),g}(\alpha^0) u_{2,j}^{(2),g}(r, \Omega) = v_j^g \sigma_{f,i_j}^g \sum_{g'=1}^G \chi^{g'} \xi_0^{(1),g'}(r), \quad j = 1, \dots, J_n; g = 1, \dots, G,$$

while being subject to the boundary conditions shown in Equations (80) and (82). Due to symmetry, the results obtained in Equation (52) for $\left(\frac{\partial^2 L}{\partial n_j \partial n_{m_2}}\right)^{(3)} = \left[\frac{\partial^2 L}{\partial t_{l_{ot}+j} \partial f_{l_{of}+l_v+m_2}}\right]_{t=N, f=N}$ must equal to those obtained in Equation (84) for $\left(\frac{\partial^2 L}{\partial n_j \partial n_{m_2}}\right)^{(9)} = \left[\frac{\partial^2 L}{\partial f_{l_{of}+l_v+j} \partial t_{l_{ot}+m_2}}\right]_{f=N, t=N}$.

The contribution stemming from the macroscopic fission and scattering cross sections is obtained by particularizing Equation (178) in [7] to the PERP benchmark, which yields:

$$\begin{aligned} \left(\frac{\partial^2 L}{\partial n_j \partial n_{m_2}}\right)^{(10)} &= \left[\frac{\partial^2 L}{\partial f_{l_{of}+l_v+j} \partial s_{l_{os}+m_2}}\right]_{f=N, s=N} \\ &= \sum_{g=1}^G \int_V dV \int_{4\pi} d\Omega u_{1,j}^{(2),g}(r, \Omega) \sum_{g'=1}^G \int_{4\pi} d\Omega' \psi^{(1),g'}(r, \Omega') \frac{\partial \Sigma_s^{g \rightarrow g'}(s; \Omega \rightarrow \Omega')}{\partial n_{m_2}} \\ &+ \sum_{g=1}^G \int_V dV \int_{4\pi} d\Omega u_{2,j}^{(2),g}(r, \Omega) \sum_{g'=1}^G \int_{4\pi} d\Omega' \varphi^{g'}(r, \Omega') \frac{\partial \Sigma_s^{g' \rightarrow g}(s; \Omega' \rightarrow \Omega)}{\partial n_{m_2}}, \end{aligned} \tag{87}$$

for $j = 1, \dots, J_n; m_2 = 1, \dots, J_n$.

Inserting Equations (44) and (45) into Equation (87) and performing the respective angular integrations yields the following simplified expression for Equation (87):

$$\begin{aligned} \left(\frac{\partial^2 L}{\partial n_j \partial n_{m_2}}\right)^{(10)} &= \left[\frac{\partial^2 L}{\partial f_{l_{of}+l_v+j} \partial s_{l_{os}+m_2}}\right]_{f=N, s=N} \\ &= \sum_{g=1}^G \sum_{l=0}^{ISCT} (2l+1) \int_V dV U_{1,j;l}^{(2),g}(r) \sum_{g'=1}^G \sigma_{s,l,m_2}^{g \rightarrow g'} \xi_l^{(1),g'}(r) + \sum_{g=1}^G \sum_{l=0}^{ISCT} (2l+1) \int_V dV U_{2,j;l}^{(2),g}(r) \sum_{g'=1}^G \sigma_{s,l,m_2}^{g' \rightarrow g} \varphi_l^{g'}(r), \end{aligned} \tag{88}$$

for $j = 1, \dots, J_n; m_2 = 1, \dots, J_n$.

where:

$$U_{1,j;l}^{(2),g}(r) \triangleq \int_{4\pi} d\Omega P_l(\Omega) u_{1,j}^{(2),g}(r, \Omega), \tag{89}$$

$$U_{2,j;l}^{(2),g}(r) \triangleq \int_{4\pi} d\Omega P_l(\Omega) u_{2,j}^{(2),g}(r, \Omega). \tag{90}$$

The contribution stemming from the macroscopic fission cross sections is obtained by particularizing Equation (179) in [7] to the PERP benchmark, which yields:

$$\begin{aligned} \left(\frac{\partial^2 L}{\partial n_j \partial n_{m_2}}\right)^{(11)} &= \left[\frac{\partial^2 L}{\partial f_{l_{of}+l_v+j} \partial f_{l_{of}+l_v+m_2}}\right]_{f=N, f=N} \\ &= \sum_{g=1}^G \int_V dV \int_{4\pi} d\Omega \psi^{(1),g}(r, \Omega) \sum_{g'=1}^G \int_{4\pi} d\Omega' \varphi^{g'}(r, \Omega') \chi^g(r) \frac{\partial^2 [(\nu \Sigma_f)^{g'}(f)]}{\partial n_j \partial n_{m_2}} \\ &+ \sum_{g=1}^G \int_V dV \int_{4\pi} d\Omega u_{1,j}^{(2),g}(r, \Omega) \frac{\partial [(\nu \Sigma_f)^g(f)]}{\partial n_{m_2}} \sum_{g'=1}^G \int_{4\pi} d\Omega' \chi^{g'} \psi^{(1),g'}(r, \Omega') \\ &+ \sum_{g=1}^G \int_V dV \int_{4\pi} d\Omega u_{2,j}^{(2),g}(r, \Omega) \sum_{g'=1}^G \int_{4\pi} d\Omega' \varphi^{g'}(r, \Omega') \chi^g \frac{\partial [(\nu \Sigma_f)^{g'}(f)]}{\partial n_{m_2}}, \end{aligned} \tag{91}$$

for $j = 1, \dots, J_n; m_2 = 1, \dots, J_n$.

Noting that:

$$\frac{\partial^2 [(\nu \Sigma_f)^{g'}(f)]}{\partial n_j \partial n_{m_2}} = \frac{\partial^2 [(\nu \Sigma_f)^{g'}(f)]}{\partial N_{i_j, m_j} \partial N_{i_{m_2}, m_{m_2}}} = 0, \tag{92}$$

and inserting Equations (50), (51) and (92) into Equation (91) yields:

$$\begin{aligned} \left(\frac{\partial^2 L}{\partial n_j \partial n_{m_2}}\right)^{(11)} &= \sum_{g=1}^G \int_V dV \nu_{i_{m_2}}^g \sigma_{f,i_{m_2}}^g U_{1,j;0}^{(2),g}(r) \sum_{g'=1}^G \chi^{g'} \xi_0^{(1),g'}(r) + \sum_{g=1}^G \int_V dV \chi^g U_{2,j;0}^{(2),g}(r) \sum_{g'=1}^G \nu_{i_{m_2}}^{g'} \sigma_{f,i_{m_2}}^{g'} \varphi_0^{g'}(r), \end{aligned} \tag{93}$$

for $j = 1, \dots, J_n; m_2 = 1, \dots, J_n$,

where:

$$U_{1,j;0}^{(2),g}(r) \triangleq \int_{4\pi} d\Omega u_{1,j}^{(2),g}(r, \Omega), \tag{94}$$

$$U_{2,j0}^{(2),g}(r) \triangleq \int_{4\pi} d\Omega u_{2,j}^{(2),g}(r, \Omega). \tag{95}$$

The contribution stemming from the macroscopic fission cross sections and the source term is obtained by particularizing Equation (181) in [7] for the PERP benchmark, which yields:

$$\left(\frac{\partial^2 L}{\partial n_j \partial n_{m_2}}\right)^{(12)} = \left[\frac{\partial^2 L}{\partial f_{\sigma_f + j \nu + j \partial q_{lq+m_2}}} \right]_{f=N, q=N} = \sum_{g=1}^G \int_V dV \int_{4\pi} d\Omega u_{2,j}^{(2),g}(r, \Omega) \frac{\partial Q^g(\mathbf{q}; r, \Omega)}{\partial n_{m_2}}, \tag{96}$$

for $j = 1, \dots, J_n; m_2 = 1, \dots, J_n$.

Inserting Equation (56) into Equation (96) yields the following expression:

$$\left(\frac{\partial^2 L}{\partial n_j \partial n_{m_2}}\right)^{(12)} = \frac{1}{n_{m_2}} \sum_{g=1}^G \int_V dV U_{2,j0}^{(2),g}(r) Q_{SF,im_2}^g, \quad j = 1, \dots, J_n; m_2 = 1, \dots, J_n. \tag{97}$$

The contribution stemming from the source term and macroscopic total cross sections is obtained by particularizing Equation (204) in [7] for the PERP benchmark, which yields:

$$\left(\frac{\partial^2 L}{\partial n_j \partial n_{m_2}}\right)^{(13)} = \left[\frac{\partial^2 L}{\partial q_{lq+j \partial t_{lot+m_2}}} \right]_{q=N, t=N} = - \sum_{g=1}^G \int_V dV \int_{4\pi} d\Omega g_{1,j}^{(2),g}(r, \Omega) \psi^{(1),g}(r, \Omega) \frac{\partial \Sigma_t^g(\mathbf{t})}{\partial n_{m_2}}, \tag{98}$$

for $j = 1, \dots, J_n; m_2 = 1, \dots, J_n$.

where the 2nd-level adjoint functions, $g_{1,j}^{(2),g}, j = 1, \dots, J_n; g = 1, \dots, G$, are the solutions of the following 2nd-Level Adjoint Sensitivity System presented in Equations (200) and (202) of [7]:

$$B^g(\alpha^0) g_{1,j}^{(2),g}(r, \Omega) = \frac{\partial Q^g(\mathbf{q}; r, \Omega)}{\partial n_j}, \quad j = 1, \dots, J_n; g = 1, \dots, G, \tag{99}$$

$$g_{1,j}^{(2),g}(r_d, \Omega) = 0, \quad \Omega \cdot \mathbf{n} < 0; j = 1, \dots, J_n; g = 1, \dots, G. \tag{100}$$

Inserting Equations (28) and (38) into Equations (99) and (98) reduces the latter equation to the following expression:

$$\left(\frac{\partial^2 L}{\partial n_j \partial n_{m_2}}\right)^{(13)} = - \sum_{g=1}^G \int_V dV \sigma_{t,im_2}^g \int_{4\pi} d\Omega g_{1,j}^{(2),g}(r, \Omega) \psi^{(1),g}(r, \Omega), \quad j = 1, \dots, J_n; m_2 = 1, \dots, J_n, \tag{101}$$

where the 2nd-level adjoint functions, $g_{1,j}^{(2),g}, j = 1, \dots, J_n; g = 1, \dots, G$, are the solutions of the following particular forms of Equation (99):

$$B^g(\alpha^0) g_{1,j}^{(2),g}(r, \Omega) = \frac{Q_{SF,ij}^g}{n_j}, \quad j = 1, \dots, J_n; g = 1, \dots, G, \tag{102}$$

subject to the boundary conditions shown in Equation (100). Due to symmetry, the results obtained from Equation (57) for $\left(\frac{\partial^2 L}{\partial n_j \partial n_{m_2}}\right)^{(4)} = \left[\frac{\partial^2 L}{\partial t_{lot+j \partial q_{lq+m_2}}} \right]_{t=N, q=N}$ must equal to that obtained from Equation (101) for $\left(\frac{\partial^2 L}{\partial n_j \partial n_{m_2}}\right)^{(13)} = \left[\frac{\partial^2 L}{\partial q_{lq+j \partial t_{lot+m_2}}} \right]_{q=N, t=N}$.

The contribution stemming from the source term and macroscopic scattering cross sections is obtained by particularizing Equation (205) in [7] to the PERP benchmark, which yields:

$$\begin{aligned} \left(\frac{\partial^2 L}{\partial n_j \partial n_{m_2}}\right)^{(14)} &= \left[\frac{\partial^2 L}{\partial q_{lq+j \partial s_{los+m_2}}} \right]_{q=N, s=N} \\ &= \sum_{g=1}^G \int_V dV \int_{4\pi} d\Omega g_{1,j}^{(2),g}(r, \Omega) \sum_{g'=1}^G \int_{4\pi} d\Omega' \psi^{(1),g'}(r, \Omega') \frac{\partial \Sigma_s^{g \rightarrow g'}(\mathbf{s}; \Omega \rightarrow \Omega')}{\partial n_{m_2}}, \quad j = 1, \dots, J_n; m_2 = 1, \dots, J_n. \end{aligned} \tag{103}$$

Inserting Equation (44) into Equation (103) and performing the respective angular integrations yields the following expression for Equation (103):

$$\left(\frac{\partial^2 L}{\partial n_j \partial n_{m_2}}\right)^{(14)} = \sum_{g=1}^G \sum_{l=0}^{ISCT} (2l+1) \int_V dV G_{1,j;l}^{(2),g}(r) \sum_{g'=1}^G \sigma_{s,l,i_{m_2}}^{g \rightarrow g'} \xi_l^{(1),g'}(r), \quad j = 1, \dots, J_n; m_2 = 1, \dots, J_n, \quad (104)$$

where:

$$G_{1,j;l}^{(2),g}(r) \triangleq \int_{4\pi} d\Omega P_l(\Omega) g_{1,j}^{(2),g}(r, \Omega). \quad (105)$$

Due to symmetry, the result obtained in Equation (77) for $\left(\frac{\partial^2 L}{\partial n_j \partial n_{m_2}}\right)^{(8)} = \left[\frac{\partial^2 L}{\partial s_{j\sigma s + j} \partial q_{lq + m_2}}\right]_{s=N, q=N}$ must equal to that obtained in Equation (104) for $\left(\frac{\partial^2 L}{\partial n_j \partial n_{m_2}}\right)^{(14)} = \left[\frac{\partial^2 L}{\partial q_{lq + j} \partial s_{j\sigma s + m_2}}\right]_{q=N, s=N}$.

The contribution stemming from the source term and macroscopic fission cross sections is obtained by particularizing Equation (206) in [7] for the PERP benchmark, which yields:

$$\begin{aligned} \left(\frac{\partial^2 L}{\partial n_j \partial n_{m_2}}\right)^{(15)} &= \left[\frac{\partial^2 L}{\partial q_{lq + j} \partial f_{j\sigma f + l\nu + m_2}}\right]_{q=N, f=N} \\ &= \sum_{g=1}^G \int_V dV \int_{4\pi} d\Omega g_{1,j}^{(2),g}(r, \Omega) \frac{\partial[(v\Sigma_f)^g(\mathbf{f})]}{\partial n_{m_2}} \sum_{g'=1}^G \int_{4\pi} d\Omega' \chi^{g'} \psi^{(1),g'}(r, \Omega'), \quad j = 1, \dots, J_n; m_2 = 1, \dots, J_n. \end{aligned} \quad (106)$$

Inserting Equation (50) into Equation (106) and performing the respective angular integrations yields the following simplified expression for Equation (106):

$$\left(\frac{\partial^2 L}{\partial n_j \partial n_{m_2}}\right)^{(15)} = \sum_{g=1}^G \int_V dV v_{m_2}^g \sigma_{f,i_{m_2}}^g G_{1,j;0}^{(2),g}(r) \sum_{g'=1}^G \chi^{g'} \xi_0^{(1),g'}(r), \quad j = 1, \dots, J_n; m_2 = 1, \dots, J_n. \quad (107)$$

Due to symmetry, the result obtained in Equation (97) for $\left(\frac{\partial^2 L}{\partial n_j \partial n_{m_2}}\right)^{(12)} = \left[\frac{\partial^2 L}{\partial f_{j\sigma f + l\nu + j} \partial q_{lq + m_2}}\right]_{f=N, q=N}$ must equal to that obtained in Equation (107) for $\left(\frac{\partial^2 L}{\partial n_j \partial n_{m_2}}\right)^{(15)} = \left[\frac{\partial^2 L}{\partial q_{lq + j} \partial f_{j\sigma f + l\nu + m_2}}\right]_{q=N, f=N}$.

Finally, the contribution stemming from the source term is obtained by particularizing Equation (208) in [7] for the PERP benchmark, which yields:

$$\begin{aligned} \left(\frac{\partial^2 L}{\partial n_j \partial n_{m_2}}\right)^{(16)} &= \left[\frac{\partial^2 L}{\partial q_{lq + j} \partial q_{lq + m_2}}\right]_{q=N, q=N} = \sum_{g=1}^G \int_V dV \int_{4\pi} d\Omega \psi^{(1),g}(r, \Omega) \frac{\partial Q^g(\mathbf{q}; r, \Omega)}{\partial n_j \partial n_{m_2}}, \\ &\text{for } j = 1, \dots, J_n; m_2 = 1, \dots, J_n. \end{aligned} \quad (108)$$

Since:

$$\frac{\partial Q^g(\mathbf{q}; r, \Omega)}{\partial n_j \partial n_{m_2}} = \frac{\partial Q^g(\mathbf{q}; r, \Omega)}{\partial N_{j,m} \partial N_{m_2,m'}} = 0, \quad (109)$$

it follows that the contribution from Equation (108) vanishes, i.e.,

$$\left(\frac{\partial^2 L}{\partial n_j \partial n_{m_2}}\right)^{(16)} = 0, \quad j = 1, \dots, J_n; m_2 = 1, \dots, J_n. \quad (110)$$

Collecting the partial contributions obtained in Equations (40), (46), (52), (57), (64), (69), (73), (77), (84), (88), (93), (97), (101), (104), (107) and (110) yields the following result:

$$\begin{aligned}
 \frac{\partial^2 L}{\partial n_j \partial n_{m_2}} &= \sum_{i=1}^{16} \left(\frac{\partial^2 L}{\partial n_j \partial n_{m_2}} \right)^{(i)} = - \sum_{g=1}^G \int_V dV \int_{4\pi} d\Omega \left[\psi_{1,j}^{(2),g}(r, \Omega) \psi^{(1),g}(r, \Omega) + \psi_{2,j}^{(2),g}(r, \Omega) \varphi^g(r, \Omega) \right] \sigma_{t,im_2}^g \\
 &+ \sum_{g=1}^G \sum_{l=0}^{ISCT} (2l+1) \int_V dV \xi_{1,j;l}^{(2),g}(r) \sum_{g'=1}^G \sigma_{s,l,im_2}^{g \rightarrow g'} \xi_l^{(1),g'}(r) + \sum_{g=1}^G \sum_{l=0}^{ISCT} (2l+1) \int_V dV \xi_{2,j;l}^{(2),g}(r) \sum_{g'=1}^G \sigma_{s,l,im_2}^{g' \rightarrow g} \varphi_l^{g'}(r) \\
 &+ \sum_{g=1}^G \int_V dV \chi^g \xi_{2,j;0}^{(2),g}(r) \sum_{g'=1}^G v_{im_2}^{g'} \sigma_{f,im_2}^{g'} \varphi_0^{g'}(r) + \sum_{g=1}^G \int_V dV v_{im_2}^g \sigma_{f,im_2}^g \xi_{1,j;0}^{(2),g}(r) \sum_{g'=1}^G \chi^{g'} \xi_0^{(1),g'}(r) \\
 &+ \frac{1}{n_{m_2}} \sum_{g=1}^G \int_V dV \xi_{2,j;0}^{(2),g}(r) Q_{SF,im_2}^g - \sum_{g=1}^G \int_V dV \sigma_{t,im_2}^g \int_{4\pi} d\Omega \left[\theta_{1,j}^{(2),g}(r, \Omega) \psi^{(1),g}(r, \Omega) + \theta_{2,j}^{(2),g}(r, \Omega) \varphi^g(r, \Omega) \right] \\
 &+ \sum_{g=1}^G \sum_{l=0}^{ISCT} (2l+1) \int_V dV \Theta_{1,j;l}^{(2),g}(r) \sum_{g'=1}^G \sigma_{s,l,im_2}^{g \rightarrow g'} \xi_l^{(1),g'}(r) + \sum_{g=1}^G \sum_{l=0}^{ISCT} (2l+1) \int_V dV \Theta_{2,j;l}^{(2),g}(r) \sum_{g'=1}^G \sigma_{s,l,im_2}^{g' \rightarrow g} \varphi_l^{g'}(r) \\
 &+ \sum_{g=1}^G \int_V dV v_{im_2}^g \sigma_{f,im_2}^g \Theta_{1,j;0}^{(2),g}(r) \sum_{g'=1}^G \chi^{g'} \xi_0^{(1),g'}(r) + \sum_{g=1}^G \int_V dV \chi^g \Theta_{2,j;0}^{(2),g}(r) \sum_{g'=1}^G v_{im_2}^{g'} \sigma_{f,im_2}^{g'} \varphi_0^{g'}(r) \\
 &+ \frac{1}{n_{m_2}} \sum_{g=1}^G \int_V dV \Theta_{2,j;0}^{(2),g}(r) Q_{SF,im_2}^g - \sum_{g=1}^G \int_V dV \int_{4\pi} d\Omega \left[u_{1,j}^{(2),g}(r, \Omega) \psi^{(1),g}(r, \Omega) + u_{2,j}^{(2),g}(r, \Omega) \varphi^g(r, \Omega) \right] \sigma_{t,im_2}^g \\
 &+ \sum_{g=1}^G \sum_{l=0}^{ISCT} (2l+1) \int_V dV U_{1,j;l}^{(2),g}(r) \sum_{g'=1}^G \sigma_{s,l,im_2}^{g \rightarrow g'} \xi_l^{(1),g'}(r) + \sum_{g=1}^G \sum_{l=0}^{ISCT} (2l+1) \int_V dV U_{2,j;l}^{(2),g}(r) \sum_{g'=1}^G \sigma_{s,l,im_2}^{g' \rightarrow g} \varphi_l^{g'}(r) \\
 &+ \sum_{g=1}^G \int_V dV v_{im_2}^g \sigma_{f,im_2}^g U_{1,j;0}^{(2),g}(r) \sum_{g'=1}^G \chi^{g'} \xi_0^{(1),g'}(r) + \sum_{g=1}^G \int_V dV \chi^g U_{2,j;0}^{(2),g}(r) \sum_{g'=1}^G v_{im_2}^{g'} \sigma_{f,im_2}^{g'} \varphi_0^{g'}(r) \\
 &+ \frac{1}{n_{m_2}} \sum_{g=1}^G \int_V dV U_{2,j;0}^{(2),g}(r) Q_{SF,im_2}^g - \sum_{g=1}^G \int_V dV \sigma_{t,im_2}^g \int_{4\pi} d\Omega g_{1,j}^{(2),g}(r, \Omega) \psi^{(1),g}(r, \Omega) \\
 &+ \sum_{g=1}^G \sum_{l=0}^{ISCT} (2l+1) \int_V dV G_{1,j;l}^{(2),g}(r) \sum_{g'=1}^G \sigma_{s,l,im_2}^{g \rightarrow g'} \xi_l^{(1),g'}(r) + \sum_{g=1}^G \int_V dV v_{im_2}^g \sigma_{f,im_2}^g G_{1,j;0}^{(2),g}(r) \sum_{g'=1}^G \chi^{g'} \xi_0^{(1),g'}(r), \\
 \text{for } j &= 1, \dots, J_n; m_2 = 1, \dots, J_n.
 \end{aligned} \tag{111}$$

The numerical values of the 2nd-order absolute sensitivities $\partial^2 L / \partial N_{i,m} \partial N_{k,m'}$, $i, k = 1, \dots, I$; $m, m' = 1, \dots, M$, where $I = 6$ and $M = 2$, of the PERP benchmark's leakage response with respect to the isotopic number densities are computed using Equation (111). The matrix $\partial^2 L / \partial N_{i,m} \partial N_{k,m'}$, $i, k = 1, \dots, 6$; $m, m' = 1, 2$ of 2nd-order absolute sensitivities has dimensions $J_n \times J_n (= 6 \times 6)$. For convenient comparisons, the numerical results presented in this Sub-section are presented in unit-less values of the relative sensitivities that correspond to $\partial^2 L / \partial N_{i,m} \partial N_{k,m'}$, $i, k = 1, \dots, 6$; $m, m' = 1, 2$, which are denoted as $S^{(2)}(N_{i,m}, N_{k,m'})$ and are defined as follows:

$$S^{(2)}(N_{i,m}, N_{k,m'}) \triangleq \frac{\partial^2 L}{\partial N_{i,m} \partial N_{k,m'}} \left(\frac{N_{i,m} N_{k,m'}}{L} \right), \quad i, k = 1, \dots, 6; \quad m, m' = 1, 2. \tag{112}$$

The numerical results obtained for the matrix $S^{(2)}(N_{i,m}, N_{k,m'})$, $i, k = 1, \dots, 6$; $m, m' = 1, 2$ are presented in Table 2. This matrix is symmetrical with respect to its principal diagonal.

Table 2. Second-order relative sensitivities of the leakage response with respect to the isotope number densities $S^{(2)}(N_{i,m}, N_{k,m'})$, $i, k = 1, \dots, 6$; $m, m' = 1, 2$.

Isotopes	k=1 (²³⁹ Pu)	k=2 (²⁴⁰ Pu)	k=3 (⁶⁹ Ga)	k=4 (⁷¹ Ga)	k=5 (C)	k=6 (¹ H)
i = 1 (²³⁹ Pu)	$S^{(2)}(N_{1,1}, N_{1,1})$ = 7.380×10^1	$S^{(2)}(N_{1,1}, N_{2,1})$ = 8.751×10^0	$S^{(2)}(N_{1,1}, N_{3,1})$ = 3.034×10^{-2}	$S^{(2)}(N_{1,1}, N_{4,1})$ = 1.917×10^{-2}	$S^{(2)}(N_{1,1}, N_{5,2})$ = 8.054×10^0	$S^{(2)}(N_{1,1}, N_{6,2})$ = 1.282×10^1
i = 2 (²⁴⁰ Pu)	$S^{(2)}(N_{2,1}, N_{1,1})$ = 8.751×10^0	$S^{(2)}(N_{2,1}, N_{2,1})$ = 5.758×10^{-1}	$S^{(2)}(N_{2,1}, N_{3,1})$ = 3.332×10^{-3}	$S^{(2)}(N_{2,1}, N_{4,1})$ = 2.061×10^{-3}	$S^{(2)}(N_{2,1}, N_{5,2})$ = 9.111×10^{-1}	$S^{(2)}(N_{2,1}, N_{6,2})$ = 1.420×10^0
i = 3 (⁶⁹ Ga)	$S^{(2)}(N_{3,1}, N_{1,1})$ = 3.035×10^{-2}	$S^{(2)}(N_{3,1}, N_{2,1})$ = 3.332×10^{-3}	$S^{(2)}(N_{3,1}, N_{3,1})$ = 1.167×10^{-5}	$S^{(2)}(N_{3,1}, N_{4,1})$ = 7.750×10^{-6}	$S^{(2)}(N_{3,1}, N_{5,2})$ = 2.707×10^{-3}	$S^{(2)}(N_{3,1}, N_{6,2})$ = 4.429×10^{-3}
i = 4 (⁷¹ Ga)	$S^{(2)}(N_{4,1}, N_{1,1})$ = 1.917×10^{-2}	$S^{(2)}(N_{4,1}, N_{2,1})$ = 2.061×10^{-3}	$S^{(2)}(N_{4,1}, N_{3,1})$ = 7.750×10^{-6}	$S^{(2)}(N_{4,1}, N_{4,1})$ = 1.154×10^{-5}	$S^{(2)}(N_{4,1}, N_{5,2})$ = 1.561×10^{-3}	$S^{(2)}(N_{4,1}, N_{6,2})$ = 2.499×10^{-3}
i = 5 (C)	$S^{(2)}(N_{5,2}, N_{1,1})$ = 8.055×10^0	$S^{(2)}(N_{5,2}, N_{2,1})$ = 9.112×10^{-1}	$S^{(2)}(N_{5,2}, N_{3,1})$ = 2.707×10^{-3}	$S^{(2)}(N_{5,2}, N_{4,1})$ = 1.561×10^{-3}	$S^{(2)}(N_{5,2}, N_{5,2})$ = 8.212×10^{-1}	$S^{(2)}(N_{5,2}, N_{6,2})$ = 1.345×10^0
i = 6 (¹ H)	$S^{(2)}(N_{6,2}, N_{1,1})$ = 1.283×10^1	$S^{(2)}(N_{6,2}, N_{2,1})$ = 1.420×10^0	$S^{(2)}(N_{6,2}, N_{3,1})$ = 4.429×10^{-3}	$S^{(2)}(N_{6,2}, N_{4,1})$ = 2.499×10^{-3}	$S^{(2)}(N_{6,2}, N_{5,2})$ = 1.345×10^0	$S^{(2)}(N_{6,2}, N_{6,2})$ = 1.912×10^0

As indicated in Table 2, all $J_n \times J_n = 36$ elements of the matrix $S^{(2)}(N_{i,m}, N_{k,m'})$ are positive, and 12 of these sensitivities are large, having values greater than 1.0. These large sensitivities involve the isotopic number densities of either ^{239}Pu or ^1H , and the isotopic number densities of ^{240}Pu or C. The largest element is the unmixed 2nd-order sensitivity with respect to the isotopic number density of ^{239}Pu , i.e., $S^{(2)}(N_{1,1}, N_{1,1}) = 7.380 \times 10^1$. On the other hand, the results shown in Table 2 indicate that all of the mixed 2nd-order relative sensitivities involving the isotopic number densities of ^{69}Ga or ^{71}Ga have absolute values smaller than 1.0.

The 2nd-order unmixed sensitivities $S^{(2)}(N_{i,m}, N_{i,m}) \triangleq (\partial^2 L / \partial N_{i,m} \partial N_{i,m})(N_{i,m} N_{i,m} / L)$, $i = 1, \dots, 6$; $m = 1, 2$, which are the elements on the diagonal of the matrix $S^{(2)}(N_{i,m}, N_{k,m'})$, $i, k = 1, \dots, 6$; $m, m' = 1, 2$, can be directly compared to the values of the 1st-order relative sensitivities $S^{(1)}(N_{i,m}) \triangleq (\partial L / \partial N_{i,m})(N_{i,m} / L)$, $i = 1, \dots, 6$; $m = 1, 2$, of the leakage response with respect to the isotopic number density parameters. Table 3 compares the 1st- and the unmixed 2nd-order relative sensitivities for all six isotopes. This comparison indicates that the values of the 2nd-order unmixed sensitivities with respect to the isotopic number densities of isotopes ^{239}Pu , C and ^1H , are 1100%, 30% and 90% larger than the corresponding values of the 1st-order sensitivities for the same isotope, respectively. The largest 1st-order relative sensitivity is $S^{(1)}(N_{1,1}) = 5.963$ while the largest 2nd-order unmixed relative sensitivity is $S^{(2)}(N_{1,1}, N_{1,1}) = 73.80$; both involve the isotopic number density of ^{239}Pu . It is noteworthy that all of the 1st-order relative sensitivities are positive, signifying that an increase in the isotopic number density will cause an increase in the total neutron leakage from the PERP sphere.

Table 3. Comparison of 1st-order relative sensitivities $(\partial L / \partial N_{i,m})(N_{i,m} / L)$, $i = 1, \dots, 6$; $m = 1, 2$ and unmixed 2nd-order relative sensitivities $(\partial^2 L / \partial N_{i,m} \partial N_{i,m})(N_{i,m} N_{i,m} / L)$, $i = 1, \dots, 6$; $m = 1, 2$ for all isotopes.

Isotopes	1st-Order	2nd-Order
$i = 1$ (^{239}Pu)	5.963×10^0	7.380×10^1
$i = 2$ (^{240}Pu)	1.220×10^0	5.758×10^{-1}
$i = 3$ (^{69}Ga)	2.229×10^{-3}	1.167×10^{-5}
$i = 4$ (^{71}Ga)	1.365×10^{-3}	1.154×10^{-5}
$i = 5$ (C)	6.312×10^{-1}	8.212×10^{-1}
$i = 6$ (^1H)	1.001×10^0	1.912×10^0

4. Quantification of Uncertainties in the PERP Leakage Response due to Uncertainties in Isotopic Number Densities

Correlations between the isotopic number densities or correlations between these isotopic number densities and other cross section parameters are not available for the PERP benchmark. When such correlations are unavailable, the maximum entropy principle [14] indicates that neglecting them minimizes the inadvertent introduction of spurious information into the computations of the various moments of the response's distribution in parameter space. The formulas for computing the expected value, variance and skewness of the response distribution by considering the 2nd-order response sensitivities together with the standard deviations of the isotopic number densities parameter correlations are as follows:

- (1) The expected value, $[E(L)]_N$, of the leakage response $L(\alpha)$ has the following expression:

$$[E(L)]_N = L(\alpha^0) + [E(L)]_N^{(2,U)}, \quad (113)$$

where the subscript "N" indicates contributions solely from the isotopic number densities, and where the 2nd-order contributions from uncorrelated isotopic number densities, denoted as $[E(L)]_N^{(2,U)}$, has the following expression:

$$[E(L)]_N^{(2,U)} = \frac{1}{2} \sum_{m=1}^M \sum_{i=1}^I \frac{\partial^2 L(\alpha)}{\partial N_{i,m} \partial N_{i,m}} (s_{N_{i,m}})^2, \quad I = 6, M = 2. \quad (114)$$

The quantity $s_{N_{i,m}}$ which appears in Equation (114) denotes the standard deviation associated with the imprecisely known model parameter $N_{i,m}$.

- (2) Since correlations among parameters are unavailable, the following formulas pertain solely to uncorrelated and normally-distributed isotopic number densities, a restriction that will be indicated by using the superscript “(U, N).” Under these restrictions, the expression for computing the variance, denoted as $[\text{var}(L)]_N^{(U,N)}$ of the PERP leakage response has the following form:

$$[\text{var}(L)]_N^{(U,N)} = [\text{var}(L)]_N^{(1,U,N)} + [\text{var}(L)]_N^{(2,U,N)}, \quad (115)$$

where the first-order contribution term, $[\text{var}(L)]_N^{(1,U,N)}$, to the variance $[\text{var}(L)]_N^{(U,N)}$ is defined as follows:

$$[\text{var}(L)]_N^{(1,U,N)} \triangleq \sum_{m=1}^M \sum_{i=1}^I \left[\frac{\partial L(\alpha)}{\partial N_{i,m}} \right]^2 (s_{N_{i,m}})^2, \quad I = 6, M = 2. \quad (116)$$

The second-order contribution term, $[\text{var}(L)]_N^{(2,U,N)}$, to the variance $[\text{var}(L)]_N^{(U,N)}$ in Equation (115) is defined as:

$$[\text{var}(L)]_N^{(2,U,N)} \triangleq \frac{1}{2} \sum_{m=1}^M \sum_{i=1}^I \left[\frac{\partial^2 L(\alpha)}{\partial N_{i,m} \partial N_{i,m}} (s_{N_{i,m}})^2 \right]^2, \quad I = 6, M = 2. \quad (117)$$

- (3) Considering uncorrelated normally-distributed isotopic number densities, the third-order moment, $[\mu_3(L)]_N^{(U,N)}$, of the leakage response for the PERP benchmark has the expression:

$$[\mu_3(L)]_N^{(U,N)} = 3 \sum_{m=1}^M \sum_{i=1}^I \left[\frac{\partial L(\alpha)}{\partial N_{i,m}} \right]^2 \frac{\partial^2 L(\alpha)}{\partial N_{i,m} \partial N_{i,m}} (s_{N_{i,m}})^4, \quad I = 6, M = 2. \quad (118)$$

As Equation (118) indicates, if the 2nd-order sensitivities were unavailable, the third moment $[\mu_3(L)]_N^{(U,N)}$ would vanish and the response distribution would by default be assumed to be Gaussian.

- (4) The skewness, $[\gamma_1(L)]_N^{(U,N)}$, in the leakage response which stems from the variances of isotopic number densities is defined as follows:

$$[\gamma_1(L)]_N^{(U,N)} = [\mu_3(L)]_N^{(U,N)} / \left\{ [\text{var}(L)]_N^{(U,N)} \right\}^{3/2}. \quad (119)$$

The effects of the first- and second-order sensitivities on the response's expected value, variance and skewness are quantified by using Equations (114) through (119) in conjunction the sensitivities computed in Sections 2 and 3 and using illustrative values of 1%, 5%, and 10%, respectively, for the standard deviations for the uncorrelated isotopic number densities. The results thus obtained are presented in Table 4.

Table 4. Comparison of Response Moments Induced by Various Relative Standard Deviations Assumed for the Parameters $N_{i,m}$.

Relative Standard Deviation	10%	5%	1%
$L(\alpha^0)$	1.7648×10^6	1.7648×10^6	1.7648×10^6
$[E(L)]_N^{(2,U)}$	6.8042×10^5	1.7011×10^5	6.8042×10^3
$[E(L)]_N = L(\alpha^0) + [E(L)]_N^{(2,U)}$	2.4452×10^6	1.9349×10^6	1.7716×10^6
$[\text{var}(L)]_N^{(1,U,N)}$	1.1993×10^{12}	2.9983×10^{11}	1.1993×10^{10}
$[\text{var}(L)]_N^{(2,U,N)}$	8.4892×10^{11}	5.3075×10^{10}	8.4892×10^7
$[\text{var}(L)]_N^{(U,N)} = [\text{var}(L)]_N^{(1,U,N)} + [\text{var}(L)]_N^{(2,U,N)}$	2.0482×10^{12}	3.5289×10^{11}	1.2078×10^{10}
$[\mu_3(L)]_N^{(U,N)}$	4.3399×10^{18}	2.7125×10^{17}	4.3399×10^{14}
$[\gamma_1(L)]_N^{(U,N)} = [\mu_3(L)]_N^{(U,N)} / \{[\text{var}(L)]_N^{(U,N)}\}^{3/2}$	1.481	1.294	0.327

The relative effects of uncertainties in the isotopic number densities can be compared to the corresponding effects stemming from the total and, respectively, fission cross sections, by considering standard deviations of 10% for all of these cross sections and by comparing the corresponding results shown in Table 4 with the corresponding results presented in Table 25 of Part I [1] and Table 27 of Part III [3]. This comparison reveals that the following relations hold:

$$\begin{aligned}
 [E(L)]_f^{(2,U)} &= 3.7191 \times 10^4 \ll [E(L)]_N^{(2,U)} = 6.8042 \times 10^5 \ll [E(L)]_i^{(2,U)} = 4.5980 \times 10^6, \\
 [\text{var}(L)]_f^{(1,U,N)} &= 9.5932 \times 10^{10} \ll [\text{var}(L)]_N^{(1,U,N)} = 1.1993 \times 10^{12} < [\text{var}(L)]_i^{(1,U,N)} = 3.4196 \times 10^{12}, \\
 [\text{var}(L)]_f^{(2)} &= 5.4830 \times 10^8 \ll [\text{var}(L)]_N^{(2)} = 8.4892 \times 10^{11} \ll [\text{var}(L)]_i^{(2)} = 2.8789 \times 10^{13}, \\
 [\gamma_1(L)]_f^{(U,N)} &= 0.1172 < [\gamma_1(L)]_i^{(U,N)} = 0.3407 \ll [\gamma_1(L)]_N^{(U,N)} = 1.481.
 \end{aligned}$$

The above relations indicate that the contributions to the expected value and variance stemming from the uncorrelated isotopic number densities are much smaller than the corresponding contributions stemming from the group-averaged uncorrelated microscopic total cross sections, but are much greater than the corresponding contributions stemming from the group-averaged uncorrelated microscopic fission cross sections. However, the contributions to the skewness stemming from the uncorrelated isotopic number densities are much larger than the corresponding contributions stemming from the group-averaged uncorrelated microscopic total and fission cross sections.

It is important to note that the results presented in Table 4 consider only the standard deviations of the isotopic number densities, since correlations between these parameters are unavailable. In the absence of parameter correlations, the possible contributions stemming from the mixed 2nd-order sensitivities involving the isotopic number densities cannot be accounted for. Recall that the results presented in Section 3 of this work and Ref. [5] indicated that a significant number of mixed 2nd-order sensitivities involving the isotopic number densities have absolute values larger than 1.0, including:

- (a) 12 elements of the matrix $S^{(2)}(N_{i,m}, N_{k,m'})$, $i, k = 1, \dots, 6$; $m, m' = 1, 2$;
- (b) 125 elements of the matrix $S^{(2)}(N_{i,m}, \sigma_{i,k}^g)$, $i, k = 1, \dots, 6$; $m = 1, 2$; $g = 1, \dots, 30$;
- (c) 15 elements of the matrix $S^{(2)}(N_{i,m}, \sigma_{s,l=0,k}^{g' \rightarrow g})$, $i, k = 1, \dots, 6$; $m = 1, 2$; $g', g = 1, \dots, 30$;
- (d) 7 elements of the matrix $S^{(2)}(N_{i,m}, \sigma_{s,l=1,k}^{g' \rightarrow g})$, $i, k = 1, \dots, 6$; $m = 1, 2$; $g', g = 1, \dots, 30$;
- (e) 21 elements of the matrix $S^{(2)}(N_{i,m}, \sigma_{f,k}^g)$, $i = 1, \dots, 6$; $k, m = 1, 2$; $g = 1, \dots, 30$;
- (f) 34 elements of the matrix $S^{(2)}(N_{i,m}, \nu_k^g)$, $i = 1, \dots, 6$; $k, m = 1, 2$; $g = 1, \dots, 30$.

The effects of the large sensitivities mentioned above on the uncertainties in the response distribution cannot be considered until the corresponding correlations among the various model parameters become available.

5. Computation of 1st-Order Sensitivities of the PERP Leakage Response with Respect to Fission Spectrum Parameters

The fission spectrum is considered to depend on the vector of parameters \mathbf{p} , which were defined in Part I [1] and are reproduced below:

$$\mathbf{p} \triangleq [p_1, \dots, p_{J_p}]^\dagger \triangleq [\chi_{i=1}^{g=1}, \chi_{i=1}^{g=2}, \dots, \chi_{i=1}^G, \dots, \chi_i^g, \dots, \chi_{N_f}^G]^\dagger, i = 1, \dots, N_f; g = 1, \dots, G; J_p = G \times N_f. \tag{120}$$

In Equation (120), the quantity χ_i^g denotes the fission spectrum of isotope i in group g . The first-order sensitivities $\partial L(\alpha)/\partial p_j, j = 1, \dots, J_p$, of the PERP leakage response to the fission spectrum parameters are computed using the following particular form of Equation (153) in [7]:

$$\frac{\partial L(\alpha)}{\partial p_j} = \sum_{g=1}^G \int_V dV \int_{4\pi} d\Omega \psi^{(1),g}(r, \Omega) \sum_{g'=1}^G \int_{4\pi} d\Omega' \frac{\partial \chi_i^g}{\partial p_j} (v\sigma_f)^{g'} \varphi^{g'}(r, \Omega'), j = 1, \dots, J_p, \tag{121}$$

where the quantity f_i^g denotes the corresponding spectrum weighting function and where χ^g denotes the material fission spectrum in energy group g , as has been defined in Part I [1], i.e.,

$$\chi^g \triangleq \frac{\sum_{i=1}^{N_f} \chi_i^g N_{i,m} \sum_{g'=1}^G (v\sigma_f)_i^{g'} f_i^{g'}}{\sum_{i=1}^{N_f} N_{i,m} \sum_{g'=1}^G (v\sigma_f)_i^{g'} f_i^{g'}}, \text{ with } \sum_{g=1}^G \chi_i^g = 1. \tag{122}$$

The numerical values of the 1st-order relative sensitivities, $\mathbf{S}^{(1)}(\chi_i^g) \triangleq (\partial L/\partial \chi_i^g)(\chi_i^g/L), i = 1, 2; g = 1, \dots, 30$, of the leakage response with respect to the fission spectrum parameters for the two fissionable isotopes (namely, ²³⁹Pu and ²⁴⁰Pu) contained in the PERP benchmark are presented in Tables 5 and 6, respectively.

Table 5. First-Order Relative Sensitivities $\mathbf{S}^{(1)}(\chi_{i=1}^g), g = 1, \dots, 30$.

g	Relative Sensitivities	g	Relative Sensitivities
1	2.539×10^{-4}	16	7.557×10^{-3}
2	4.642×10^{-4}	17	3.309×10^{-3}
3	1.220×10^{-3}	18	8.557×10^{-4}
4	4.836×10^{-3}	19	2.332×10^{-4}
5	1.920×10^{-2}	20	1.219×10^{-4}
6	2.601×10^{-2}	21	5.140×10^{-5}
7	-5.541×10^{-3}	22	1.180×10^{-5}
8	2.059×10^{-2}	23	4.199×10^{-6}
9	1.743×10^{-2}	24	3.010×10^{-7}
10	2.005×10^{-2}	25	2.974×10^{-7}
11	5.346×10^{-3}	26	6.408×10^{-8}
12	-5.005×10^{-2}	27	-2.804×10^{-10}
13	-4.730×10^{-2}	28	-3.975×10^{-9}
14	-2.116×10^{-2}	29	2.057×10^{-9}
15	-3.506×10^{-3}	30	1.672×10^{-9}

Table 6. First-Order Relative Sensitivities $S^{(1)}(\lambda_{i=2}^g)$, $g = 1, \dots, 30$.

g	Relative Sensitivities	g	Relative Sensitivities
1	1.671×10^{-8}	16	4.627×10^{-7}
2	3.022×10^{-8}	17	2.023×10^{-7}
3	7.797×10^{-8}	18	5.245×10^{-8}
4	3.037×10^{-7}	19	1.425×10^{-8}
5	1.187×10^{-6}	20	7.480×10^{-9}
6	1.595×10^{-6}	21	3.174×10^{-9}
7	-3.390×10^{-7}	22	7.361×10^{-10}
8	1.253×10^{-6}	23	2.657×10^{-10}
9	1.061×10^{-6}	24	1.941×10^{-11}
10	1.222×10^{-6}	25	1.966×10^{-11}
11	3.254×10^{-7}	26	4.419×10^{-12}
12	-3.062×10^{-6}	27	-2.031×10^{-14}
13	-2.900×10^{-6}	28	-2.953×10^{-13}
14	-1.299×10^{-6}	29	1.545×10^{-13}
15	-2.154×10^{-7}	30	1.260×10^{-13}

The values presented in Table 5 for the 1st-order relative sensitivities of the leakage response with respect to the fission spectrum parameters of ^{239}Pu are all very small, the largest being of the order of 10^{-2} . Similarly, as shown in Table 6, the 1st-order relative sensitivities of the leakage response with respect to the fission spectrum of ^{240}Pu are even smaller, largest being of the order of 10^{-6} . Based on the results that have been presented in Part I–Part III [1–3] for the 1st-order and 1st-order relative sensitivities of the leakage response with respect to the parameters underlying the total, scattering, fission microscopic cross sections and average number of neutrons per fission, and in view of the small values of the 1st-order relative sensitivities presented in Tables 5 and 6, it can be inferred that the 2nd-order relative sensitivities of the leakage response with respect to the fission spectrum parameters of isotopes ^{239}Pu and ^{240}Pu would be very small. This inference has been confirmed by sample computations of 2nd-order sensitivities of the PERP leakage response with respect to fission spectrum parameters. For the sake of brevity, these computations will not be presented herein.

6. Overall Conclusions: Ranking and Impact of the First- and Second-Order Sensitivities of the PERP Benchmark’s Leakage Response with Respect to the Benchmark’s 21976 Imprecisely Known Parameters

This Section presents the overall summary and conclusions based on the comprehensive results that have been detailed in Parts I–V [1–5] and in the present work for the 1st- and 2nd-order sensitivities of the PERP benchmark’s leakage response with respect to (all 21976 of) the PERP model’s imprecisely known parameters. To begin with, Table 7 presents a summary of the magnitudes attained by the 1st-order relative sensitivities of the PERP benchmark’s leakage response, which indicates that the largest 13 of these sensitivities attain values between 1.0 and 10.0; all others are smaller than 1.0. Of these 13 large sensitivities, 8 involve the total microscopic group cross sections, 3 involve the isotopic number densities (of ^{239}Pu , ^{240}Pu , and ^1H ; see Table 3 in this work), 1 involves the average number of neutrons produced per fission of ^{239}Pu , and 1 involves a source parameter. Additional details regarding these large 1st-order relative sensitivities (which involve nuclear data pertaining to ^{239}Pu , ^{240}Pu , and ^1H) of the PERP benchmark’s leakage response are further discussed below in comparison to the corresponding 2nd-order unmixed sensitivities.

Table 8 presents the summary of the 2nd-order mixed relative sensitivities of the PERP benchmark’s leakage response having absolute values greater than 1.0. Since Table 8 is symmetrical, the upper triangular submatrices are not shown in the table; of course, each of the upper triangular submatrices has the same number of large sensitivities as its symmetrical counterpart. Table 8 indicates that 126 2nd-order relative sensitivities have values greater than 10.0, and 1853 2nd-order relative sensitivities have values between 1.0 and 10.0. Evidently, the number of 2nd-order relative sensitivities having

values greater than 1.0 is far larger than the number of 1st-order relative sensitivities that have values greater than 1.0.

Table 7. Summary of the large 1st-order relative sensitivities for the PERP benchmark.

$S^{(1)}(\sigma_t)$	$S^{(1)}(\sigma_s)$	$S^{(1)}(\sigma_f)$	$S^{(1)}(\nu)$	$S^{(1)}(q)$	$S^{(1)}(p)$	$S^{(1)}(N)$
$n_{1-10} = 8,$ $n_{>10.0} = 0$	$n_{1-10} = 0,$ $n_{>10.0} = 0$	$n_{1-10} = 0,$ $n_{>10.0} = 0$	$n_{1-10} = 1,$ $n_{>10.0} = 0$	$n_{1-10} = 1,$ $n_{>10.0} = 0$	$n_{1-10} = 0,$ $n_{>10.0} = 0$	$n_{1-10} = 3,$ $n_{>10.0} = 0$

Note: (1) n_{1-10} denotes the total number of elements with absolute values between [1.0,10.0]; (2) $n_{>10.0}$ denotes the total number of elements with absolute values greater than 10.0.

Table 8. Summary of the large 2nd-order relative sensitivities for the PERP benchmark.

Parameters	σ_t	σ_s	σ_f	ν	q	N
σ_t	$S^{(2)}(\sigma_t, \sigma_t)$ $n_{1-10} = 665$ $n_{>10.0} = 55$					
σ_s	$S^{(2)}(\sigma_s, \sigma_t)$ $n_{1-10} = 52$ $n_{>10.0} = 1$	$S^{(2)}(\sigma_s, \sigma_s)$ $n_{1-10} = 0$ $n_{>10.0} = 0$				
σ_f	$S^{(2)}(\sigma_f, \sigma_t)$ $n_{1-10} = 83$ $n_{>10.0} = 1$	$S^{(2)}(\sigma_f, \sigma_s)$ $n_{1-10} = 0$ $n_{>10.0} = 0$	$S^{(2)}(\sigma_f, \sigma_f)$ $n_{1-10} = 11$ $n_{>10.0} = 0$			
ν	$S^{(2)}(\nu, \sigma_t)$ $n_{1-10} = 171$ $n_{>10.0} = 8$	$S^{(2)}(\nu, \sigma_s)$ $n_{1-10} = 0$ $n_{>10.0} = 0$	$S^{(2)}(\nu, \sigma_f)$ $n_{1-10} = 28$ $n_{>10.0} = 0$	$S^{(2)}(\nu, \nu)$ $n_{1-10} = 52$ $n_{>10.0} = 0$		
q	$S^{(2)}(q, \sigma_t)$ $n_{1-10} = 32$ $n_{>10.0} = 0$	$S^{(2)}(q, \sigma_s)$ $n_{1-10} = 0$ $n_{>10.0} = 0$	$S^{(2)}(q, \sigma_f)$ $n_{1-10} = 0$ $n_{>10.0} = 0$	$S^{(2)}(q, \nu)$ $n_{1-10} = 4$ $n_{>10.0} = 0$	$S^{(2)}(q, q)$ $n_{1-10} = 0$ $n_{>10.0} = 0$	
N	$S^{(2)}(N, \sigma_t)$ $n_{1-10} = 108$ $n_{>10.0} = 17$	$S^{(2)}(N, \sigma_s)$ $n_{1-10} = 23$ $n_{>10.0} = 0$	$S^{(2)}(N, \sigma_f)$ $n_{1-10} = 20$ $n_{>10.0} = 1$	$S^{(2)}(N, \nu)$ $n_{1-10} = 28$ $n_{>10.0} = 6$	$S^{(2)}(N, q)$ $n_{1-10} = 9$ $n_{>10.0} = 0$	$S^{(2)}(N, N)$ $n_{1-10} = 9$ $n_{>10.0} = 3$

Note: (1) n_{1-10} denotes the total number of elements with absolute values between [1.0,10.0]; (2) $n_{>10.0}$ denotes the total number of elements with absolute values greater than 10.0.

The results detailed in Parts I–V [1–5] and in the present work have indicated that the largest 1st- and unmixed 2nd-order sensitivities of the PERP benchmark's leakage response are with respect to the nuclear parameters related to ^{239}Pu . Figure 2 presents the comparison of the absolute values of the 1st-order relative sensitivities, for each of the 30 energy groups, of the PERP benchmark's leakage response with respect to the following groups of imprecisely known parameters related to ^{239}Pu : (i) the total microscopic cross sections [1]; (ii) the scattering microscopic cross sections [2]; (iii) fission microscopic cross sections [3]; (iv) the average number of neutrons per fission [3]; (v) the source parameters [4]; and (vi) the fission spectrum, as presented in Table 5 in this work. As Figure 2 indicates, the 1st-order relative sensitivities of the PERP's leakage response with respect to the imprecisely known parameters related to ^{239}Pu can be ranked in the following order of importance:

- (i) The 1st-order relative sensitivities $S^{(1)}(\sigma_{t,1}^g)$ of the leakage response with respect to the total cross sections of ^{239}Pu have the largest magnitudes for all energy groups;
- (ii) The next largest magnitudes are displayed by the 1st-order relative sensitivities $S^{(1)}(\nu_1^g)$ with respect to the average number of neutrons per fission of ^{239}Pu . The values of these 1st-order sensitivities are about 30% to 50% larger than those corresponding to the fission cross sections, which follow next in the importance ranking.

- (iii) The third largest are the 1st-order relative sensitivities $s^{(1)}(\sigma_{f,1}^g)$ of the PERP benchmark's leakage response with respect to the fission cross sections of ^{239}Pu .
- (iv) The fourth largest are the 1st-order relative sensitivities $s^{(1)}(\sigma_{s,l=0,1}^{g \rightarrow g})$ of the leakage response with respect to the 0th-order self-scattering cross sections for ^{239}Pu . These 1st-order relative sensitivities are approximately one order of magnitude smaller than the corresponding 1st-order relative sensitivities with respect to the fission cross sections of ^{239}Pu .
- (v) The next-to-last in the importance ranking are the 1st-order relative sensitivities $s^{(1)}(\chi_1^g)$ of the leakage response with respect to the fission spectrum parameters;
- (vi) Finally, the 1st-order relative sensitivities $s^{(1)}(q_1^g)$ of the leakage response with respect to the source parameters of ^{239}Pu are the smallest of the sensitivities pertaining to ^{239}Pu .

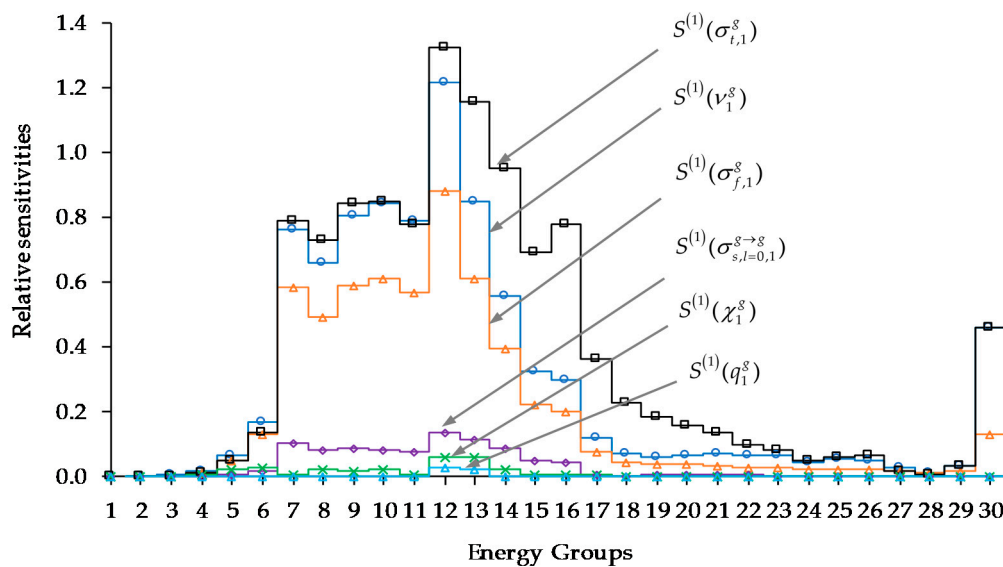


Figure 2. Comparison of first-order relative sensitivities for isotope 1 (^{239}Pu).

The largest 2nd-order unmixed sensitivities of the PERP benchmark's leakage response also involve the imprecisely known parameters pertaining to ^{239}Pu . Based on the results presented in Parts I–III [1–3], Figure 3 illustrates the importance ranking for the absolute values of the unmixed 2nd-order relative sensitivities with respect to the parameters underlying the total, scattering and fission cross sections, and the average number of neutrons per fission of ^{239}Pu .

The results presented in Figure 3 highlight the following features:

- (i) For every energy group, the 2nd-order unmixed sensitivities with respect to the total cross sections are the largest and significantly larger than any others.
- (ii) The 2nd-order unmixed sensitivities with respect to the parameters underlying the average number of neutrons per fission are the second largest, being approximately 100–200% larger than the 2nd-order unmixed sensitivities with respect to the fission cross sections.
- (iii) The 2nd-order unmixed sensitivities with respect to scattering cross sections are negligibly small comparing to others.
- (iv) Comparing the results shown in Figures 2 and 3 reveals the important conclusion that the 2nd-order unmixed sensitivities of the leakage response with respect to the microscopic total group cross sections of ^{239}Pu are significantly (over 300–400%) larger than the corresponding 1st-order sensitivities.

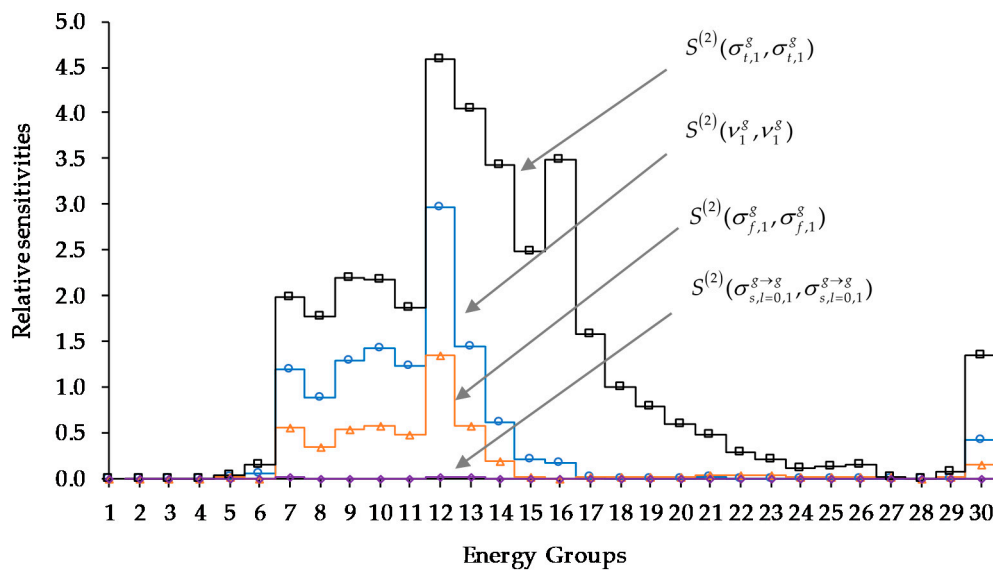


Figure 3. Comparison of second-order relative sensitivities for isotope 1 (²³⁹Pu).

The next largest group of 1st- and 2nd-order relative sensitivities of the PERP’s leakage response pertain to parameters related to ²⁴⁰Pu, which are displayed in Figures 4 and 5. Comparing the results displayed in Figures 4 and 5 to the results presented in Figures 2 and 3 indicates that, albeit important, the sensitivities of the PERP’s leakage response to parameters pertaining to ²⁴⁰Pu are at least an order of magnitude smaller than the sensitivities pertaining to ²³⁹Pu.

The PERP benchmark’s leakage response displays remarkably large 1st- and 2nd-order sensitivities with respect to the total microscopic cross section of ¹H in the lowest-energy group. These large sensitivities are illustrated in Figures 6 and 7.

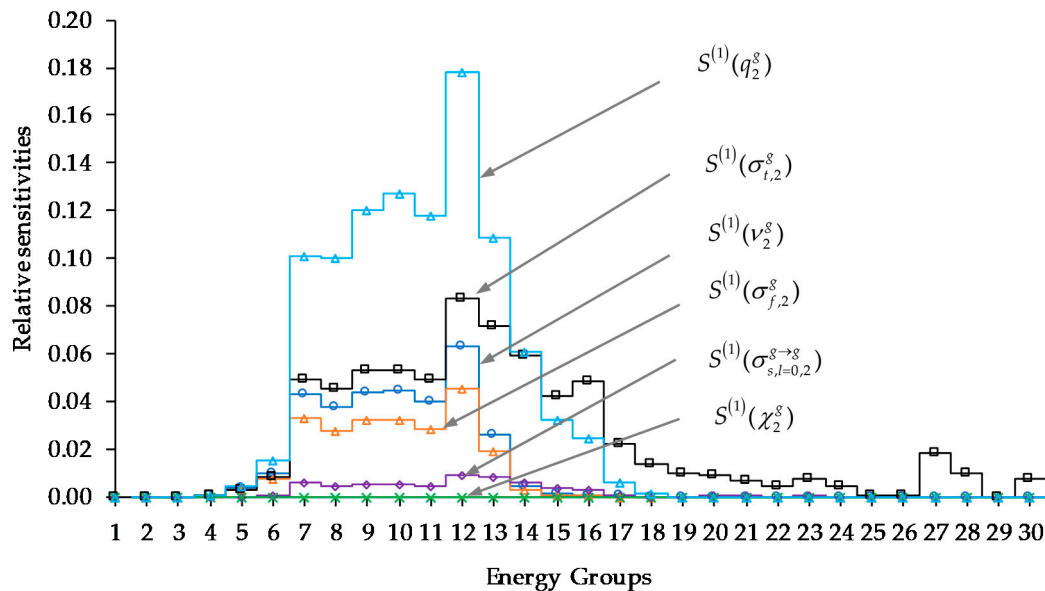


Figure 4. Comparison of first-order relative sensitivities for isotope 2 (²⁴⁰Pu).

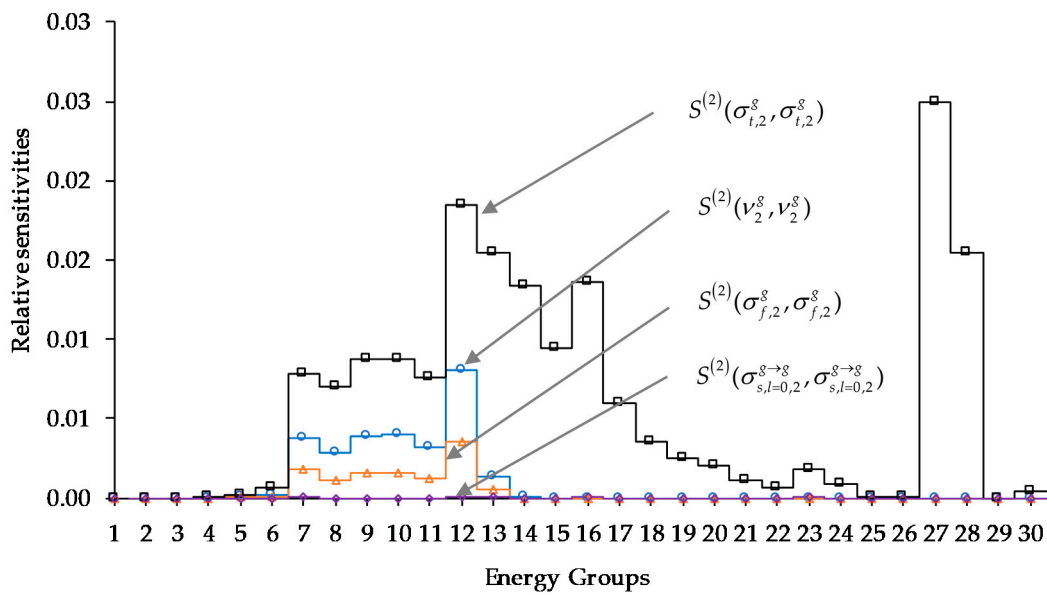


Figure 5. Comparison of second-order relative sensitivities for isotope 2 (^{240}Pu).

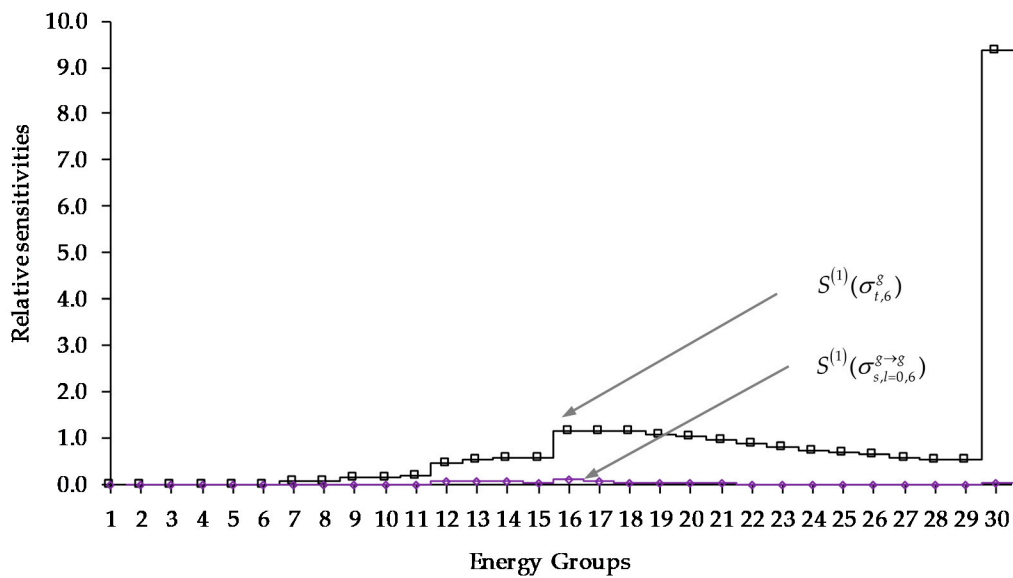


Figure 6. Comparison of first-order relative sensitivities for isotope 6 (^1H).

Figures 8–11 present comprehensive comparisons of the contributions of the 1st- and, respectively, 2nd-order sensitivities of the PERP’s leakage response to the expected values, variances and skewness of this response, considering that all of the PERP’s model parameters (fission, scattering and fission microscopic cross sections, the average number of neutrons per fission, isotopic number densities, and source parameters) are uncorrelated and have uniform standard deviations of 5% or 10%, respectively. The vertical-axes in Figures 8–11 use logarithmic scales.

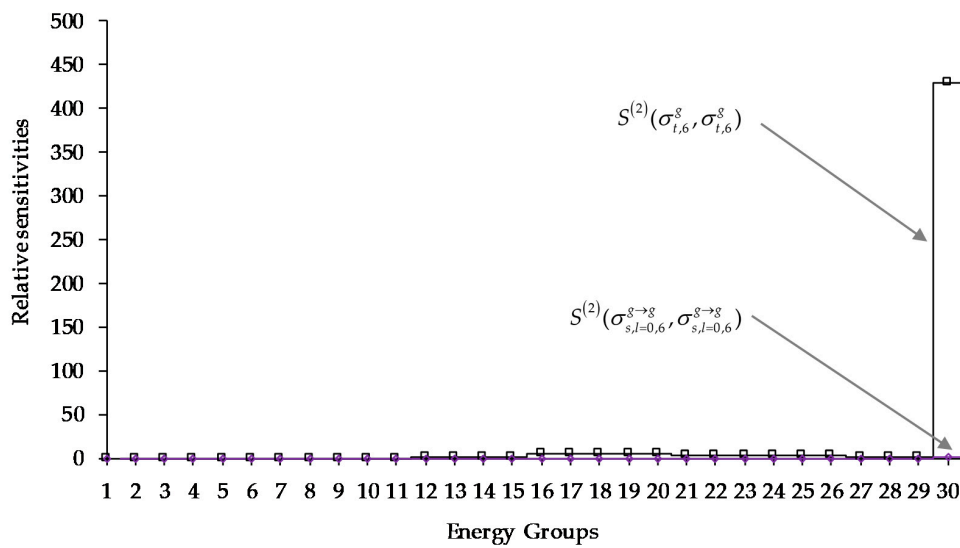


Figure 7. Comparison of second-order relative sensitivities for isotope 6 (^1H).

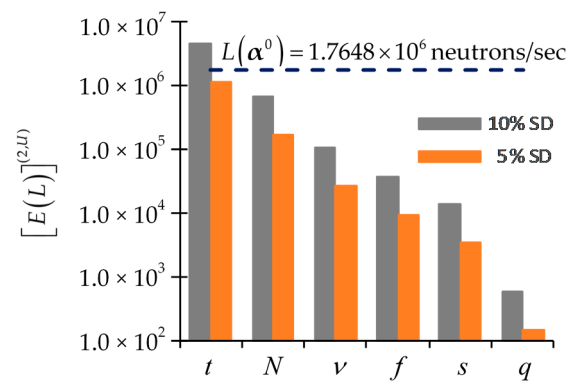


Figure 8. Contributions, $[E(L)]_i^{(2,U)}$, $i = t, N, v, f, s, q$, to the leakage response expected value, $E(L)$, stemming from 2nd-order sensitivities of the parameters (considered to be uncorrelated) underlying the total, scattering and fission cross sections, the average number of neutrons per fission, isotopic number densities, and the source parameters, for uniform 5% and 10% standard deviations (SD) respectively.

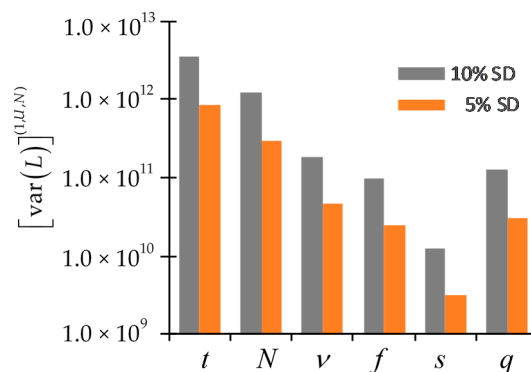


Figure 9. Comparison of $[\text{var}(L)]_i^{(1,U,N)}$, $i = t, N, v, f, s, q$, due to 5% and 10% standard deviations (SD) of the parameters (considered to be uncorrelated and normally distributed) underlying the total, scattering and fission cross sections, the average number of neutrons per fission, isotopic number densities, and the source parameters, respectively.

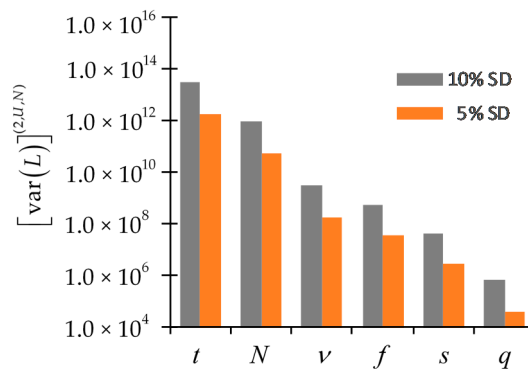


Figure 10. Comparison of $[\text{var}(L)]_i^{(2,U,N)}$, $i = t, N, v, f, s, q$, due to 5% and 10% standard deviations (SD) of the parameters (considered to be uncorrelated and normally distributed) underlying the total, scattering and fission cross sections, the average number of neutrons per fission, isotopic number densities, and the source parameters, respectively.

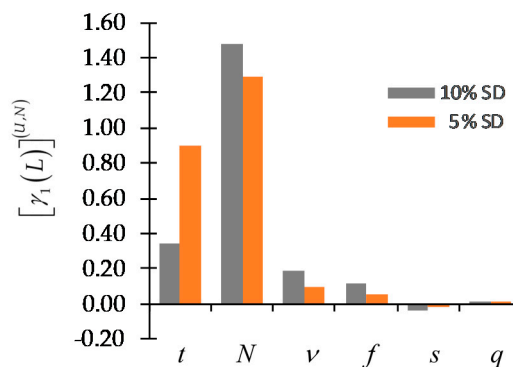


Figure 11. Comparison of $[\gamma_1(L)]_i^{(U,N)}$, $i = t, N, v, f, s, q$, due to 5% and 10% standard deviations (SD) of the parameters (considered to be uncorrelated and normally distributed) underlying the total, scattering and fission cross sections, the average number of neutrons per fission, isotopic number densities, and the source parameters, respectively.

Thus, Figure 8 illustrates the magnitudes of the 2nd-order contributions, $[E(L)]_i^{(2,U)}$, $i = t, N, v, f, s, q$, to the expected value, $E(L)$, of the PERP's leakage response. The 2nd-order contributions, $[E(L)]_i^{(2,U)}$, are computed in [1–4] using expressions similar to Equation (114) and stem from 2nd-order sensitivities of the parameters underlying the total, scattering and fission cross sections, the average number of neutrons per fission, isotopic number densities, and the source parameters, respectively. Since correlations among parameters are unavailable, these parameters are considered to be uncorrelated and having all uniform standard deviations (SD) of either 5% or 10% respectively. A standard deviation of 5% is typical for the available nuclear data while the standard deviation of 10% is used to illustrate how an increase in the parameter uncertainties would affect the expected value of the leakage response. The nominal value, $L(\alpha^0)$, of the leakage response is also displayed in Figure 8, in order to provide an evident standard for assessing the importance of the 2nd-order contributions $[E(L)]_i^{(2,U)}$ to the expected value, $E(L)$, of the PERP's leakage response. Recall from Equation (113) that if the 2nd-order sensitivities are ignored or are unavailable, the expected value, $E(L)$, will coincide with the nominal value, $L(\alpha^0)$. The comparison presented in Figure 8 indicates that, assuming a uniform standard deviation of either 5% or 10% for all parameters, the magnitudes of the 2nd-order contributions stemming from the various imprecisely known nuclear data fall into the following ranking order (from small to large):

$$[E(L)]_q^{(2,U)} \ll [E(L)]_s^{(2,U)} < [E(L)]_f^{(2,U)} < [E(L)]_v^{(2,U)} \ll [E(L)]_N^{(2,U)} \ll [E(L)]_t^{(2,U)}.$$

Figure 9 presents a comparison of contributions to the 1st-order variance, $[\text{var}(L)]_i^{(1,U,N)}$, computed using expressions similar to Equation (116), of the 1st-order sensitivities of the PERP leakage response

to the PERP parameters (considered to be uncorrelated and normally distributed) underlying the total, scattering and fission cross sections, the average number of neutrons per fission, isotopic number densities, and the source parameters, as presented in [1–4], respectively. The comparison presented in Figure 9 indicates that, assuming a uniform standard deviation of either 5% or 10% for all parameters, the magnitudes of the 2nd-order contributions stemming from the various imprecisely known nuclear data fall into the following ranking order (from small to large):

$$[\text{var}(L)]_s^{(1,U,N)} \ll [\text{var}(L)]_f^{(1,U,N)} < [\text{var}(L)]_q^{(1,U,N)} < [\text{var}(L)]_v^{(1,U,N)} \ll [\text{var}(L)]_N^{(1,U,N)} < [\text{var}(L)]_i^{(1,U,N)}.$$

Figure 10 presents a comparison of contributions to the 2nd-order variance, $[\text{var}(L)]_i^{(2,U,N)}$, computed using expressions similar to Equation (117), of the 2nd-order sensitivities of the PERP leakage response to the PERP parameters (considered to be uncorrelated and normally distributed) underlying the total, scattering and fission cross sections, the average number of neutrons per fission, isotopic number densities, and the source parameters, as presented in [1–4], respectively. The comparison presented in Figure 10 indicates that, assuming a uniform standard deviation of either 5% or 10% for all parameters, the magnitudes of the 2nd-order contributions stemming from the various imprecisely known nuclear data fall into the following ranking order (from small to large):

$$[\text{var}(L)]_q^{(2,U,N)} \ll [\text{var}(L)]_s^{(2,U,N)} \ll [\text{var}(L)]_f^{(2,U,N)} < [\text{var}(L)]_v^{(2,U,N)} \ll [\text{var}(L)]_N^{(2,U,N)} \ll [\text{var}(L)]_i^{(2,U,N)}.$$

Figure 11 presents a comparison of contributions to the skewness, $[\gamma_1(L)]_i^{(U,N)}$, computed using expressions similar to Equation (119), of the PERP leakage response to the PERP parameters (considered to be uncorrelated and normally distributed) underlying the total, scattering and fission cross sections, the average number of neutrons per fission, isotopic number densities, and the source parameters, as presented in [1–4], respectively. The comparison presented in Figure 11 indicates that, assuming a uniform standard deviation of either 5% or 10% for all parameters, the magnitudes of the 2nd-order contributions stemming from the various imprecisely known nuclear data fall into the following ranking order (from small to large):

$$[\gamma_1(L)]_s^{(U,N)} < 0 < [\gamma_1(L)]_q^{(U,N)} \ll [\gamma_1(L)]_f^{(U,N)} < [\gamma_1(L)]_v^{(U,N)} < [\gamma_1(L)]_i^{(U,N)} \ll [\gamma_1(L)]_N^{(U,N)}.$$

The results presented in Figures 8–10 indicate that the contributions to the expected values and the (1st- and 2nd-order) variances of the PERP leakage stemming from the imprecisely known PERP parameters follow the following order of importance:

- (i) The contributions stemming from the 1st- and 2nd-order sensitivities of the leakage response to the group-averaged uncorrelated total cross sections are the largest, by a significant margin, by comparison to the contributions from any of the other parameters. The contributions from the 2nd-order sensitivities are paramount, causing the following significant effects: (i) the *expected value* of the leakage response is significantly larger than the corresponding *computed value*, and (ii) $SD^{(2)} \gg SD^{(1)}$, i.e., the 2nd-order standard deviation $SD^{(2)}$ is significantly larger than the 1st-order standard deviation $SD^{(1)}$.
- (ii) The contributions stemming from the 1st- and 2nd-order sensitivities of the leakage response to the uncorrelated isotopic number densities are second in importance.
- (iii) Ranked third in importance are the contributions stemming from the 1st- and 2nd-order sensitivities of the leakage response to the average number of neutrons per fission.
- (iv) The contributions to the expected values and variances stemming from the group-averaged uncorrelated fission cross section parameters rank overall fourth in importance, even if the relation $[\text{var}(L)]_f^{(1,U,N)} < [\text{var}(L)]_q^{(1,U,N)}$ indicates that the contributions stemming from the 1st-order sensitivities of the response to the fission parameters are slightly smaller than the contributions stemming from the 1st-order response sensitivities to the source parameters.
- (v) The contributions stemming from the group-averaged uncorrelated microscopic scattering cross sections and source parameters are smaller by factors of 10^3 – 10^7 by comparison to the contributions stemming from the 1st- and 2nd-order response sensitivities with respect to the other parameters.

Notably, the results summarized in Figure 11 indicate that the contribution to the skewness stemming from the uncorrelated isotopic number densities is much larger than that stemming from

other parameters. It is also remarkable that the skewness stemming solely from the scattering microscopic group cross sections is negative, meaning that if the only imprecisely known PERP parameters were the scattering microscopic group cross sections, then the distribution of the PERP's leakage response would be skewed towards values lower than the expectation of the response. In contradistinction, the skewness arising from uncertainties in the other parameters are all positive, signifying that uncertainties in all of the other PERP model parameters would cause the distribution of the PERP's leakage response to be skewed towards values higher than the expectation of the response.

Assuming that all PERP model parameters are uncorrelated and assuming that all of these parameters have uniform relative standard deviations of 5%, Figures 12–16 present results for the following quantities: (i) the expected value $[E(L)]$ of the PERP leakage response, which takes into account the contributions stemming from the corresponding 2nd-order sensitivities; (ii) the standard deviations, $SD^{(1)}$, for the PERP leakage response arising solely from the 1st-order sensitivities (in green); (iii) the standard deviations, $SD^{(2)}$, for the PERP leakage response arising solely from the 2nd-order sensitivities; and (iv) the sum, $SD^{(1)} + SD^{(2)}$, for the PERP leakage response stemming from both the 1st- and 2nd-order sensitivities. In Figures 12–16, the green-colored plots involve solely 1st-order sensitivities, while the red-colored plots depict the contributions from 2nd-order sensitivities. Consistent with the importance rankings illustrated in Figures 8–10, the results presented in Figures 12–16 indicate that the largest effects of the 2nd-order sensitivities are displayed by the results illustrated in Figure 12 for the total microscopic cross sections, followed, in order of importance, by the contributions involving the isotopic number densities (displayed in Figure 13), and followed the contributions involving the average number of neutrons per fission (displayed in Figure 14). As indicated by the results displayed in Figures 15 and 16, the contributions stemming from the uncorrelated fission microscopic cross sections and, respectively, the scattering microscopic cross sections are negligibly small, as are the contributions stemming from the sensitivities of the leakage response with respect to the source parameters (not shown).

Figures 17–21 also present results for: (i) the expected value $[E(L)]$ of the PERP leakage response; (ii) the standard deviations, $SD^{(1)}$, for the PERP leakage response arising solely from the 1st-order sensitivities; (iii) the standard deviations, $SD^{(2)}$, for the PERP leakage response arising solely from the 2nd-order sensitivities; and (iv) the sum, $SD^{(1)} + SD^{(2)}$, for the PERP leakage response stemming from both the 1st- and 2nd-order sensitivities. As in Figures 12–16, the green-colored plots in Figures 17–21 involve solely 1st-order sensitivities, while the red-colored plots in Figures 17–21 depict the contributions from 2nd-order sensitivities. In contradistinction with the results displayed in Figures 12–16, however, the results displayed in Figures 17–21 assume that all PERP model parameters are uncorrelated and have uniform relative standard deviations of 10% (rather than 5%). Although standard deviations of 10% are rather large for nuclear data, these larger standard deviations highlight dramatically the effects of the 2nd-order sensitivities in uncertainty analysis.

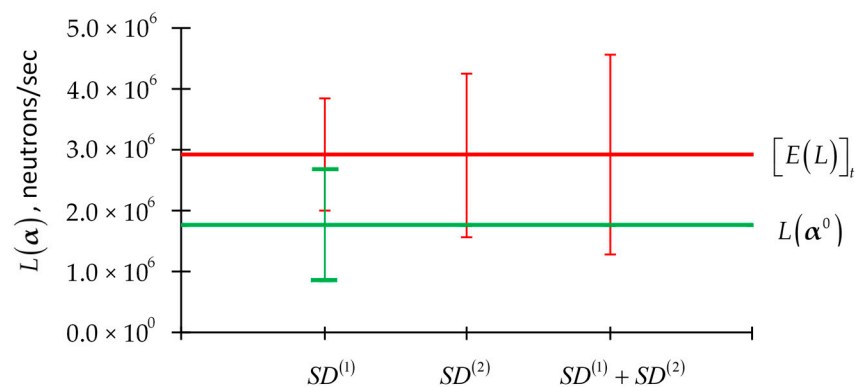


Figure 12. Comparison of $L(\alpha^0) \pm SD^{(1)}$ (in green), $[E(L)]_t \pm SD^{(1)}$, $SD^{(2)}$, $SD^{(1)} + SD^{(2)}$ (in red), due to 5% standard deviations of the uncorrelated total microscopic cross sections.

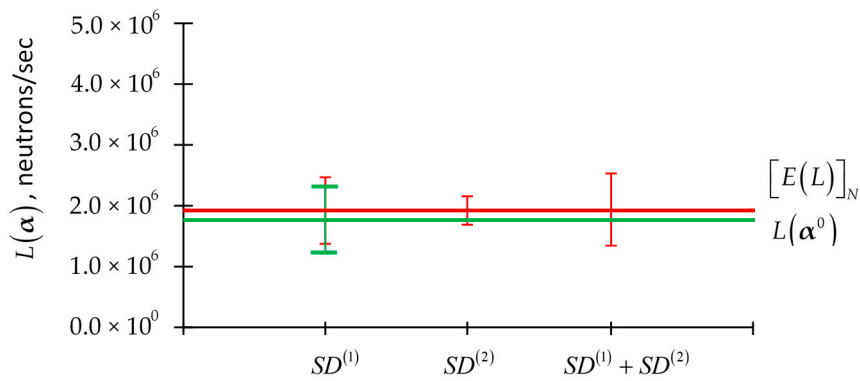


Figure 13. Comparison of $L(\alpha^0) \pm SD^{(1)}$ (in green), $[E(L)]_N \pm SD^{(1)}, SD^{(2)}, SD^{(1)} + SD^{(2)}$ (in red), due to 5% standard deviations of the uncorrelated isotopic number densities.

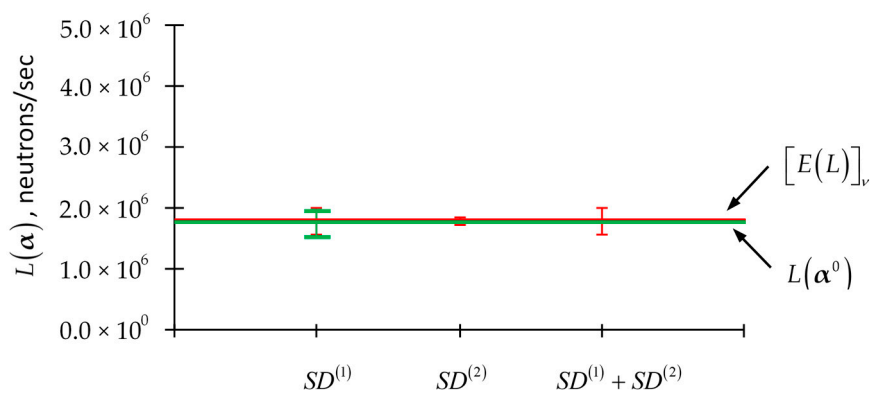


Figure 14. Comparison of $L(\alpha^0) \pm SD^{(1)}$ (in green), $[E(L)]_v \pm SD^{(1)}, SD^{(2)}, SD^{(1)} + SD^{(2)}$ (in red), due to 5% standard deviations of the parameters underlying the uncorrelated average number of neutrons per fission.

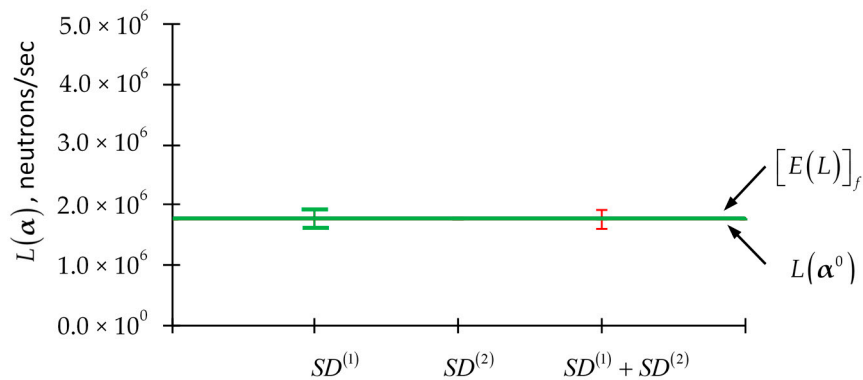


Figure 15. Comparison of $L(\alpha^0) \pm SD^{(1)}$ (in green), $[E(L)]_f \pm SD^{(1)}, SD^{(2)}, SD^{(1)} + SD^{(2)}$ (in red), due to 5% standard deviations of the parameters underlying the uncorrelated fission microscopic cross sections.

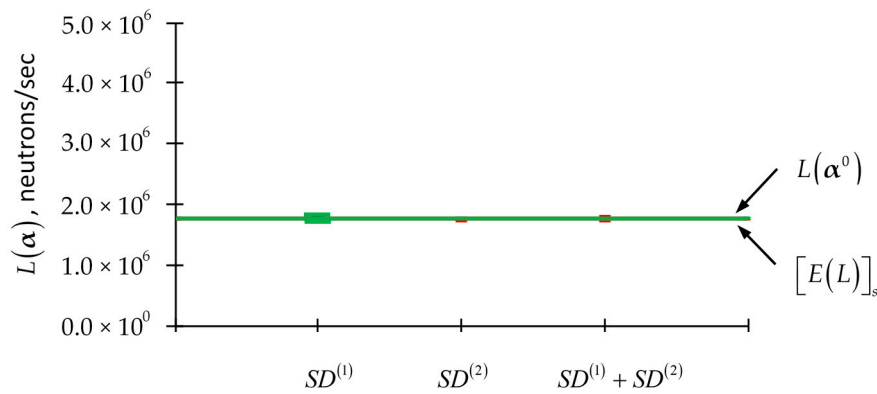


Figure 16. Comparison of $L(\alpha^0) \pm SD^{(1)}$ (in green), $[E(L)]_s \pm SD^{(1)}, SD^{(2)}, SD^{(1)} + SD^{(2)}$ (in red), due to 5% standard deviations of the parameters underlying the uncorrelated scattering microscopic cross sections.

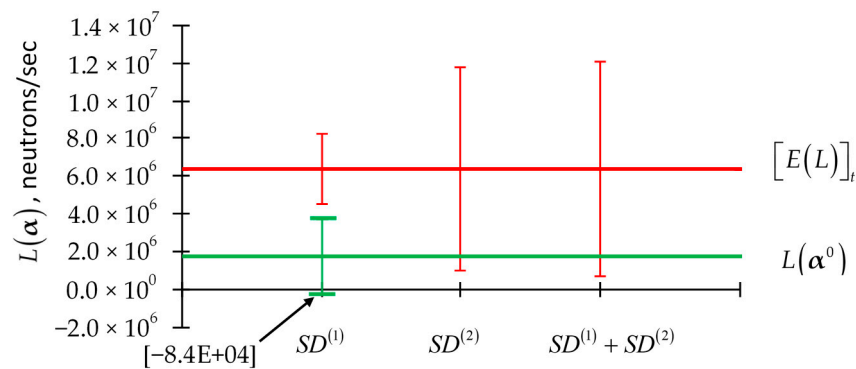


Figure 17. Comparison of $L(\alpha^0) \pm SD^{(1)}$ (in green), $[E(L)]_t \pm SD^{(1)}, SD^{(2)}, SD^{(1)} + SD^{(2)}$ (in red), due to 10% standard deviations of the uncorrelated total microscopic cross sections.

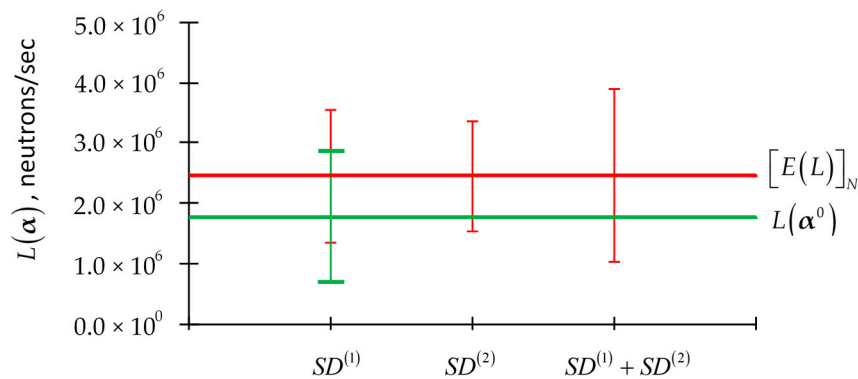


Figure 18. Comparison of $L(\alpha^0) \pm SD^{(1)}$ (in green), $[E(L)]_N \pm SD^{(1)}, SD^{(2)}, SD^{(1)} + SD^{(2)}$ (in red), due to 10% standard deviations of the uncorrelated isotopic number densities.

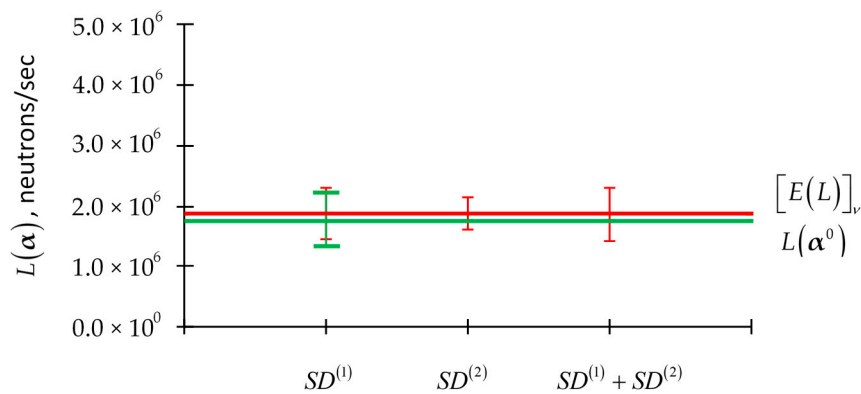


Figure 19. Comparison of $L(\alpha^0) \pm SD^{(1)}$ (in green), $[E(L)]_v \pm SD^{(1)}, SD^{(2)}, SD^{(1)} + SD^{(2)}$ (in red), due to 10% standard deviations of the parameters underlying the uncorrelated average number of neutrons per fission.

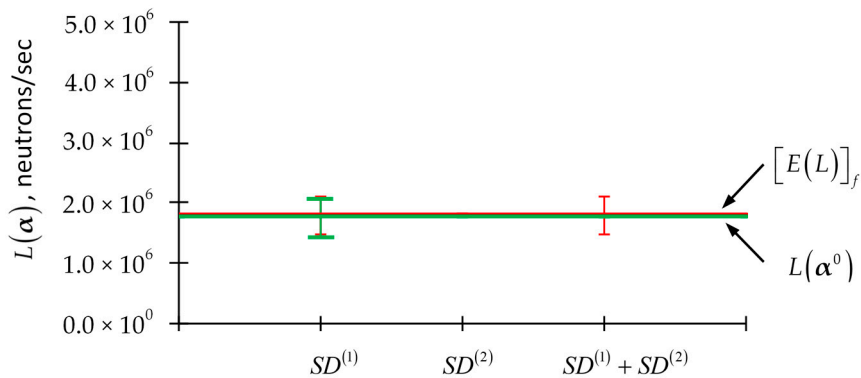


Figure 20. Comparison of $L(\alpha^0) \pm SD^{(1)}$ (in green), $[E(L)]_f \pm SD^{(1)}, SD^{(2)}, SD^{(1)} + SD^{(2)}$ (in red), due to 10% standard deviations of the parameters underlying the uncorrelated fission microscopic cross sections.

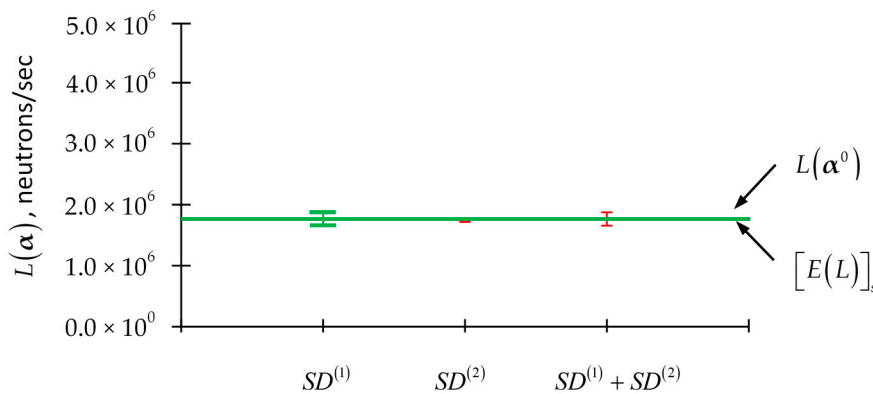


Figure 21. Comparison of $L(\alpha^0) \pm SD^{(1)}$ (in green), $[E(L)]_s \pm SD^{(1)}, SD^{(2)}, SD^{(1)} + SD^{(2)}$ (in red), due to 10% standard deviations of the parameters underlying the uncorrelated scattering microscopic cross sections.

Consistent with the importance rankings illustrated in Figures 12–16, the results presented in Figures 17–21 indicate that importance ranking of the parameter sensitivities displayed for standard deviations of 5% remains unchanged when the standard deviations are uniformly increased to 10%. Very important, however, are the results displayed in the green-colored plots in Figure 17, which

indicate that, if the 2nd-order sensitivities of the leakage response to the total microscopic group cross sections are neglected, the use of only the 1st-order sensitivities yields unphysical results, since the quantity $L(\alpha^0) - SD^{(1)}$ takes on unphysical negative values.

The sequence of works [1–5] and the present work, labeled as Parts I–VI, have applied the Second-Order Adjoint Sensitivity Analysis Methodology (2nd-ASAM) conceived by Cacuci [6,7] to compute exactly the 21,976 first-order sensitivities and 482,944,576 second-order sensitivities of a polyethylene-reflected plutonium (PERP) benchmark's leakage response with respect to the benchmark's imprecisely known parameters. The 2nd-ASAM is the only known methodology, at this time, which enables such large-scale exhaustive computations of the exact expressions of 2nd-order response sensitivities. The results of these pioneering computations have indicated that there are many 2nd-order sensitivities that have values significantly larger than the 1st-order ones. Specifically, 13 first-order sensitivities attain values between 1.0 and 10.0, while 126 second-order relative sensitivities have values greater than 10.0, and 1853 second-order relative sensitivities have values between 1.0 and 10.0. Hence, the number of 2nd-order relative sensitivities having values greater than 1.0 is obviously far larger than the number of 1st-order relative sensitivities that have values greater than 1.0.

Since correlations among the PERP's model parameters are unavailable, the effects of the 1st- and 2nd-order sensitivities in contributing to the expected value and standard deviation of the PERP's leakage response have mostly been illustrated by assuming that all model's parameters are uncorrelated. This assumption eliminates the effects of the mixed 2nd-order sensitivities. On the other hand, the illustrative results presented in Part I [1] for the extreme case of fully correlated total cross sections have shown that neglecting the 2nd-order sensitivities would cause an error as large as 2000% in the expected value of the leakage response, and up to 6000% in the variance of the leakage response for the microscopic group total cross sections. These illustrative examples have highlighted the fact that the importance of the mixed 2nd-order sensitivities increases as the respective cross sections correlations and standard deviations increase. Of course, neither the fully uncorrelated nor the fully correlated illustrative examples presented in this sequence of works [1–5] realistically describe the actual physical situations regarding the parameters describing the total and other microscopic cross section. The fully uncorrelated case underestimates reality while the fully correlated case overestimates it. In reality, cross sections are partially correlated, so reality falls in between the fully uncorrelated and fully correlated cases. Nevertheless, the illustrative examples in [1–5] underscore the need for future experimental research aimed at obtaining values for the correlations that might exist among the various cross sections, which are unavailable at this time. Correlations among the model parameters (e.g., total and fission cross sections, isotopic number densities, and the average number of neutrons per fission) provide contributions to the response distribution moments (i.e., expected values, variance, skewness, etc.) in addition to those stemming from the parameters' standard deviations.

All in all, this sequence of works [1–5] aimed at drawing attention to the fact that 2nd-order sensitivities are important, and their effects must be assessed for each physical system under consideration. For the PERP benchmark, in particular, it has been shown that the 2nd-order sensitivities are even more important than the 1st-order ones. While the effects of the 2nd-order sensitivities may be less marked for other reactor physics systems, the point is that *they are not always negligible*, as they have been a priori assumed in hitherto in the published literature. Finally, since this sequence of works [1–5] has revealed that the 2nd-order mixed relative sensitivities of the PERP benchmark's leakage response to this benchmark's total cross sections exhibit a very large number of values that are greater than 1.0 (including many having values significantly larger than 10.0), it is of clear interest to compute the magnitude of the corresponding 3rd-order sensitivities of the leakage response with respect to the parameters underlying the PERP's total cross sections. The computation of these 3rd-order sensitivities is currently under way and will be reported soon.

Author Contributions: D.G.C. conceived and directed the research reported herein, developed the general theory of the second-order comprehensive adjoint sensitivity analysis methodology to compute 1st- and 2nd-order sensitivities of flux functionals in a multiplying system with source, and the uncertainty equations for response moments. R.F. has derived the expressions of the various derivatives with respect to the model parameters to the PERP benchmark and has performed all the numerical calculations. J.A.F. has provided initial guidance to

R.F. for using PARTTSN and SOURCES4C, and has independently verified, using approximate finite-difference computations with selected perturbed parameters, several numerical results obtained by R.F. All authors have read and agreed to the published version of the manuscript.

Funding: This work was partially funded by the United States National Nuclear Security Administration’s Office of Defense Nuclear Nonproliferation Research & Development, grand number 155040-FD50.

Conflicts of Interest: The authors declare no conflict of interest. The founding sponsors had no role in the design of the study; in the collection, analyses, or interpretation of data; in the writing of the manuscript, and in the decision to publish the results.

Appendix A. Definitions of PERP Model Parameters

As presented in Part I [1], the components of the vector of 1st-order sensitivities of the leakage response with respect to the model parameters, denoted as $\mathbf{S}^{(1)}(\alpha)$, is defined as follows:

$$\mathbf{S}^{(1)}(\alpha) \triangleq \left[\frac{\partial L(\alpha)}{\partial \sigma_t}, \frac{\partial L(\alpha)}{\partial \sigma_s}, \frac{\partial L(\alpha)}{\partial \sigma_f}, \frac{\partial L(\alpha)}{\partial \nu}, \frac{\partial L(\alpha)}{\partial \mathbf{p}}, \frac{\partial L(\alpha)}{\partial \mathbf{q}}, \frac{\partial L(\alpha)}{\partial \mathbf{N}} \right]^\dagger. \tag{A1}$$

The symmetric matrix of 2nd-order sensitivities of the leakage response with respect to the model parameters, denoted as $\mathbf{S}^{(2)}(\alpha)$, is defined as follows:

$$\mathbf{S}^{(2)}(\alpha) \triangleq \begin{bmatrix} \frac{\partial^2 L(\alpha)}{\partial \sigma_t \partial \sigma_t} & * & * & * & * & * & * \\ \frac{\partial^2 L(\alpha)}{\partial \sigma_s \partial \sigma_t} & \frac{\partial^2 L(\alpha)}{\partial \sigma_s \partial \sigma_s} & * & * & * & * & * \\ \frac{\partial^2 L(\alpha)}{\partial \sigma_f \partial \sigma_t} & \frac{\partial^2 L(\alpha)}{\partial \sigma_f \partial \sigma_s} & \frac{\partial^2 L(\alpha)}{\partial \sigma_f \partial \sigma_f} & * & * & * & * \\ \frac{\partial^2 L(\alpha)}{\partial \nu \partial \sigma_t} & \frac{\partial^2 L(\alpha)}{\partial \nu \partial \sigma_s} & \frac{\partial^2 L(\alpha)}{\partial \nu \partial \sigma_f} & \frac{\partial^2 L(\alpha)}{\partial \nu \partial \nu} & * & * & * \\ \frac{\partial^2 L(\alpha)}{\partial \mathbf{p} \partial \sigma_t} & \frac{\partial^2 L(\alpha)}{\partial \mathbf{p} \partial \sigma_s} & \frac{\partial^2 L(\alpha)}{\partial \mathbf{p} \partial \sigma_f} & \frac{\partial^2 L(\alpha)}{\partial \mathbf{p} \partial \nu} & \frac{\partial^2 L(\alpha)}{\partial \mathbf{p} \partial \mathbf{p}} & * & * \\ \frac{\partial^2 L(\alpha)}{\partial \mathbf{q} \partial \sigma_t} & \frac{\partial^2 L(\alpha)}{\partial \mathbf{q} \partial \sigma_s} & \frac{\partial^2 L(\alpha)}{\partial \mathbf{q} \partial \sigma_f} & \frac{\partial^2 L(\alpha)}{\partial \mathbf{q} \partial \nu} & \frac{\partial^2 L(\alpha)}{\partial \mathbf{q} \partial \mathbf{p}} & \frac{\partial^2 L(\alpha)}{\partial \mathbf{q} \partial \mathbf{q}} & * \\ \frac{\partial^2 L(\alpha)}{\partial \mathbf{N} \partial \sigma_t} & \frac{\partial^2 L(\alpha)}{\partial \mathbf{N} \partial \sigma_s} & \frac{\partial^2 L(\alpha)}{\partial \mathbf{N} \partial \sigma_f} & \frac{\partial^2 L(\alpha)}{\partial \mathbf{N} \partial \nu} & \frac{\partial^2 L(\alpha)}{\partial \mathbf{N} \partial \mathbf{p}} & \frac{\partial^2 L(\alpha)}{\partial \mathbf{N} \partial \mathbf{q}} & \frac{\partial^2 L(\alpha)}{\partial \mathbf{N} \partial \mathbf{N}} \end{bmatrix}. \tag{A2}$$

As defined in Equation (1), the vector $\alpha \triangleq [\sigma_t; \sigma_s; \sigma_f; \nu; \mathbf{p}; \mathbf{q}; \mathbf{N}]^\dagger$ denotes the “vector of imprecisely known model parameters”, with vector-components $\sigma_t, \sigma_s, \sigma_f, \nu, \mathbf{p}, \mathbf{q}$ and \mathbf{N} , comprising the various model parameters for the microscopic total cross sections, scattering cross sections, fission cross sections, average number of neutrons per fission, fission spectra, sources, and isotopic number densities, which have been described in Part I [1]. For easy referencing, however, the definitions of these model parameters will be provided in the remainder of this Appendix.

The total cross section Σ_t^g for energy group $g, g = 1, \dots, G$, is computed for the PERP benchmark using the following expression:

$$\Sigma_t^g = \sum_{m=1}^{M=2} \Sigma_{t,m}^g; \quad \Sigma_{t,m}^g = \sum_i^I N_{i,m} \sigma_{t,i}^g = \sum_i^I N_{i,m} \left[\sigma_{f,i}^g + \sigma_{c,i}^g + \sum_{g'=1}^G \sigma_{s,l=0,i}^{g \rightarrow g'} \right], \quad m = 1, 2, \tag{A3}$$

where m denotes the materials in the PERP benchmark; $\sigma_{f,i}^g$ and $\sigma_{c,i}^g$ denote, respectively, the tabulated group microscopic fission and neutron capture cross sections for group $g, g = 1, \dots, G$. Other nuclear reactions are negligible in the PERP benchmark. As discussed in Part I [1], the total cross section $\Sigma_t^g \rightarrow \Sigma_t^g(\mathbf{t})$ will depend on the vector of parameters \mathbf{t} , which is defined as follows:

$$\mathbf{t} \triangleq [t_1, \dots, t_{J_t}]^\dagger \triangleq [t_1, \dots, t_{J_{ot}}; n_1, \dots, n_{J_n}]^\dagger \triangleq [\sigma_t; \mathbf{N}]^\dagger, \quad J_t = J_{\sigma t} + J_n, \tag{A4}$$

where:

$$\mathbf{N} \triangleq [n_1, \dots, n_{J_n}]^\dagger \triangleq [N_{1,1}, N_{2,1}, N_{3,1}, N_{4,1}, N_{5,2}, N_{6,2}]^\dagger, \quad J_n = 6, \tag{A5}$$

$$\sigma_t \triangleq [t_1, \dots, t_{J_{ot}}]^\dagger \triangleq [\sigma_{t,i=1}^1, \sigma_{t,i=1}^2, \dots, \sigma_{t,i=1}^G, \sigma_{t,i'}^1, \dots, \sigma_{t,i'=I'}^1, \dots, \sigma_{t,i=I}^G, \sigma_{t,i=I}^G]^\dagger, \tag{A6}$$

$i = 1, \dots, I = 6; \quad g = 1, \dots, G = 30; \quad J_{ot} = I \times G.$

In Equations (A4) through (A6), the dagger denotes “transposition”, $\sigma_{i,i}^g$ denotes the microscopic total cross section for isotope i and energy group g , $N_{i,m}$ denotes the respective isotopic number density, and J_n denotes the total number of isotopic number densities in the model. Thus, the vector \mathbf{t} comprises a total of $J_t = J_{ot} + J_n = 30 \times 6 + 6 = 186$ imprecisely known “model parameters” as its components.

The scattering transfer cross section $\Sigma_s^{g' \rightarrow g}(\Omega' \rightarrow \Omega)$ from energy group g' , $g' = 1, \dots, G$ into energy group g , $g = 1, \dots, G$, is computed using the finite Legendre polynomial expansion of order $ISCT = 3$:

$$\begin{aligned} \Sigma_s^{g' \rightarrow g}(\Omega' \rightarrow \Omega) &= \sum_{m=1}^{M=2} \Sigma_{s,m}^{g' \rightarrow g}(\Omega' \rightarrow \Omega), \\ \Sigma_{s,m}^{g' \rightarrow g}(\Omega' \rightarrow \Omega) &\cong \sum_{i=1}^{I=6} N_{i,m} \sum_{l=0}^{ISCT=3} (2l+1) \sigma_{s,i}^{g' \rightarrow g} P_l(\Omega' \cdot \Omega), \quad m = 1, 2, \end{aligned} \tag{A7}$$

where $\sigma_{s,i}^{g' \rightarrow g}$ denotes the l -th order Legendre-expanded microscopic scattering cross section from energy group g' into energy group g for isotope i . In view of Equation (A7), the scattering cross section $\Sigma_s^{g' \rightarrow g}(\Omega' \rightarrow \Omega) \rightarrow \Sigma_s^{g' \rightarrow g}(s; \Omega' \rightarrow \Omega)$ depends on the vector of parameters \mathbf{s} , which is defined as follows:

$$\mathbf{s} \triangleq [s_1, \dots, s_{J_s}]^\dagger \triangleq [s_1, \dots, s_{J_{os}}; n_1, \dots, n_{J_n}]^\dagger \triangleq [\sigma_s; \mathbf{N}]^\dagger, \quad J_s = J_{os} + J_n, \tag{A8}$$

$$\begin{aligned} \sigma_s \triangleq [s_1, \dots, s_{J_{os}}]^\dagger &\triangleq [\sigma_{s,l=0,i=1}^{g'=1 \rightarrow g=1}, \sigma_{s,l=0,i=1}^{g'=2 \rightarrow g=1}, \dots, \sigma_{s,l=0,i=1}^{g'=G \rightarrow g=1}, \sigma_{s,l=0,i=1}^{g'=1 \rightarrow g=2}, \sigma_{s,l=0,i=1}^{g'=2 \rightarrow g=2}, \dots, \sigma_{s,i}^{g' \rightarrow g}, \dots, \sigma_{s,ISCT,i=1}^{G \rightarrow G}]^\dagger, \\ l = 0, \dots, ISCT; \quad i = 1, \dots, I; \quad g, g' = 1, \dots, G; \quad J_{os} &= (G \times G) \times I \times (ISCT + 1). \end{aligned} \tag{A9}$$

The expressions in Equations (A7) and (A3) indicate that the zeroth order (i.e., $l = 0$) scattering cross sections must be considered separately from the higher order (i.e., $l \geq 1$) scattering cross sections, since the former contribute to the total cross sections, while the latter do not. Therefore, the total number of zeroth-order scattering cross section comprise in σ_s is denoted as $J_{os,l=0}$, where $J_{os,l=0} = G \times G \times I$; and the total number of higher order (i.e., $l \geq 1$) scattering cross sections comprised in σ_s is denoted as $J_{os,l \geq 1}$, where $J_{os,l \geq 1} = G \times G \times I \times ISCT$, with $J_{os,l=0} + J_{os,l \geq 1} = J_{os}$. Thus, the vector \mathbf{s} comprises a total of $J_{os} + J_n = 30 \times 30 \times 6 \times (3 + 1) + 6 = 21606$ imprecisely known components (“model parameters”).

The transport code PARTISN [11] computes the quantity $(v\Sigma_f)^g$ using directly the quantities $(v\sigma)_{f,i}^g$, which are provided in data files for each isotope i , and energy group g , as follows

$$(v\Sigma_f)^g = \sum_{m=1}^{M=2} (v\Sigma_f)_m^g; \quad (v\Sigma_f)_m^g = \sum_{i=1}^{I=6} N_{i,m} (v\sigma)_{f,i}^g, \quad m = 1, 2. \tag{A10}$$

In view of Equation (A10), the quantity $(v\Sigma_f)^g \rightarrow (v\Sigma_f)^g(\mathbf{f}; r)$ depends on the vector of parameters \mathbf{f} , which is defined as follows:

$$\mathbf{f} \triangleq [f_1, \dots, f_{J_{of}}; f_{J_{of}+1}, \dots, f_{J_{of}+J_v}; f_{J_{of}+J_v+1}, \dots, f_{J_f}]^\dagger \triangleq [\sigma_f; \mathbf{v}; \mathbf{N}]^\dagger, \quad J_f = J_{of} + J_v + J_n, \tag{A11}$$

where:

$$\begin{aligned} \sigma_f \triangleq [\sigma_{f,i=1}^1, \sigma_{f,i=1}^2, \dots, \sigma_{f,i=1}^G, \sigma_{f,i'}^g, \dots, \sigma_{f,i=N_f}^1, \dots, \sigma_{f,i=N_f}^G]^\dagger &\triangleq [f_1, \dots, f_{J_{of}}]^\dagger, \\ i = 1, \dots, N_f; \quad g = 1, \dots, G; \quad J_{of} &= G \times N_f, \end{aligned} \tag{A12}$$

$$\begin{aligned} \mathbf{v} \triangleq [v_{i=1}^1, v_{i=1}^2, \dots, v_{i=1}^G, v_i^g, \dots, v_{i=N_f}^1, \dots, v_{i=N_f}^G]^\dagger &\triangleq [f_{J_{of}+1}, \dots, f_{J_{of}+J_v}]^\dagger, \\ i = 1, \dots, N_f; \quad g = 1, \dots, G; \quad J_v &= G \times N_f, \end{aligned} \tag{A13}$$

and where $\sigma_{f,i}^g$ denotes the microscopic fission cross section for isotope i and energy group g , ν_i^g denotes the average number of neutrons per fission for isotope i and energy group g , and N_f denotes the total number of fissionable isotopes. For the purposes of sensitivity analysis, the quantity ν_i^g , can be obtained by using the relation $\nu_{f,i}^g = (v\sigma)_{f,i}^g / \sigma_{f,i}^g$, where the isotopic fission cross sections $\sigma_{f,i}^g$ are available in data files for computing reaction rates.

The quantity χ^g in Equation (3) quantifies the material fission spectrum in energy group g , and is defined in PARTISN [11] as follows:

$$\chi^g \triangleq \frac{\sum_{i=1}^{N_f} \chi_i^g N_{i,m} \sum_{g'=1}^G (v\sigma_f)_i^{g'} f_i^{g'}}{\sum_{i=1}^{N_f} N_{i,m} \sum_{g'=1}^G (v\sigma_f)_i^{g'} f_i^{g'}}, \text{ with } \sum_{g=1}^G \chi_i^g = 1, \quad (\text{A14})$$

where the quantity χ_i^g denotes the isotopic fission spectrum in energy group g , while the quantity f_i^g denotes the corresponding spectrum weighting function.

The fission spectrum is considered to depend on the vector of parameters \mathbf{p} , defined as follows:

$$\mathbf{p} \triangleq [p_1, \dots, p_{J_p}]^\dagger \triangleq [\chi_{i=1}^{g=1}, \chi_{i=1}^{g=2}, \dots, \chi_{i=1}^G, \dots, \chi_i^g, \dots, \chi_{N_f}^G]^\dagger, \quad i = 1, \dots, N_f; \quad g = 1, \dots, G; \quad J_p = G \times N_f. \quad (\text{A15})$$

The source $Q^g(r) \rightarrow Q^g(\mathbf{q}; \mathbf{N})$ depends on the vector of model parameters \mathbf{q} , which is defined as follows:

$$\mathbf{q} \triangleq [q_1, \dots, q_{J_q}]^\dagger \triangleq [\lambda_1, \lambda_2; F_1^{SF}, F_2^{SF}; a_1, a_2; b_1, b_2; v_1^{SF}, v_2^{SF}]^\dagger, \quad J_q = 10. \quad (\text{A16})$$

In view of Equations (A4)–(A16), the model parameters characterizing the PERP benchmark can all be considered to be the components of the following “vector of model parameters”:

$$\boldsymbol{\alpha} \triangleq [\alpha_1, \dots, \alpha_{J_\alpha}]^\dagger \triangleq [\boldsymbol{\sigma}_t; \boldsymbol{\sigma}_s; \boldsymbol{\sigma}_f; \mathbf{v}; \mathbf{p}; \mathbf{q}; \mathbf{N}]^\dagger, \quad J_\alpha = J_{\sigma_t} + J_{\sigma_s} + J_{\sigma_f} + J_v + J_p + J_q + J_n. \quad (\text{A17})$$

References

1. Cacuci, D.G.; Fang, R.; Favorite, J.A. Comprehensive second-order adjoint sensitivity analysis methodology (2nd-ASAM) applied to a subcritical experimental reactor physics benchmark: I. Effects of imprecisely known microscopic total and capture cross sections. *Energies* **2019**, *12*, 4219. [\[CrossRef\]](#)
2. Fang, R.; Cacuci, D.G. Comprehensive second-order adjoint sensitivity analysis methodology (2nd-ASAM) applied to a subcritical experimental reactor physics benchmark: II. Effects of imprecisely known microscopic scattering cross sections. *Energies* **2019**, *12*, 4114. [\[CrossRef\]](#)
3. Cacuci, D.G.; Fang, R.; Favorite, J.A.; Badea, M.C.; di Rocco, F. Comprehensive second-order adjoint sensitivity analysis methodology (2nd-ASAM) applied to a subcritical experimental reactor physics benchmark: III. Effects of imprecisely known microscopic fission cross sections and average number of neutrons per fission. *Energies* **2019**, *12*, 4100. [\[CrossRef\]](#)
4. Fang, R.; Cacuci, D.G. Comprehensive second-order adjoint sensitivity analysis methodology (2nd-ASAM) applied to a subcritical experimental reactor physics benchmark: IV. Effects of imprecisely known source parameters. *Energies* **2020**, *13*, 1431. [\[CrossRef\]](#)
5. Fang, R.; Cacuci, D.G. Comprehensive second-order adjoint sensitivity analysis methodology (2nd-ASAM) applied to a subcritical experimental reactor physics benchmark: V. Computation of mixed 2nd-Order sensitivities involving isotopic number densities. *Energies* **2020**, *13*, 1431, in press. [\[CrossRef\]](#)
6. Cacuci, D.G. *The Second-Order Adjoint Sensitivity Analysis Methodology*; CRC Press; Taylor & Francis Group: Boca Raton, FL, USA, 2018.
7. Cacuci, D.G. Application of the second-order comprehensive adjoint sensitivity analysis methodology to compute 1st- and 2nd-order sensitivities of flux functionals in a multiplying system with source. *Nucl. Sci. Eng.* **2019**, *193*, 555–600. [\[CrossRef\]](#)
8. Cacuci, D.G. Second-order sensitivities of a general functional of the forward and adjoint fluxes in a multiplying nuclear system with source. *Nucl. Eng. Des.* **2019**, *344*, 83–106. [\[CrossRef\]](#)
9. Cacuci, D.G. Second-order adjoint sensitivity analysis of a general ratio of functionals of the forward and adjoint fluxes in a multiplying nuclear system with source. *Ann. Nucl. Energy* **2020**, *135*, 106956. [\[CrossRef\]](#)
10. Valentine, T.E. *Polyethylene-Reflected Plutonium Metal Sphere Subcritical Noise Measurements, SUB-PU-METMIXED-001*; International Handbook of Evaluated Criticality Safety Benchmark Experiments; NEA/NSC/DOC(95)03/I-IX; Organization for Economic Co-Operation and Development; Nuclear Energy Agency: Paris, France, 2006.

11. Alcouffe, R.E.; Baker, R.S.; Dahl, J.A.; Turner, S.A.; Ward, R. *PARTISN: A Time-Dependent, Parallel Neutral Particle Transport Code System*; LA-UR-08-07258; Los Alamos National Laboratory: Los Alamos, NM, USA, 2008.
12. Wilson, W.B.; Perry, R.T.; Shores, E.F.; Charlton, W.S.; Parish, T.A.; Estes, G.P.; Brown, T.H.; Arthur, E.D.; Bozoian, M.; England, T.R.; et al. SOURCES4C: A code for calculating (α,n), spontaneous fission, and delayed neutron sources and spectra. In Proceedings of the American Nuclear Society/Radiation Protection and Shielding Division 12th Biennial Topical Meeting, Santa Fe, NM, USA, 14–18 April 2002.
13. Conlin, J.L.; Parsons, D.K.; Gardiner, S.J.; Beth Lee, M.G.M.; White, M.C. *MENDF71X: Multigroup Neutron Cross-Section Data Tables Based upon ENDF/B-VII.1X*; Los Alamos National Laboratory Report LA-UR-15-29571; Los Alamos National Laboratory: Los Alamos, NM, USA, 2013.
14. Cacuci, D.G. *BERRU Predictive Modeling: Best Estimate Results with Reduced Uncertainties*; Springer: Heidelberg, Germany; New York, NY, USA, 2018.



© 2020 by the authors. Licensee MDPI, Basel, Switzerland. This article is an open access article distributed under the terms and conditions of the Creative Commons Attribution (CC BY) license (<http://creativecommons.org/licenses/by/4.0/>).